Mon. Not. R. Astron. Soc. **295,** 549–567 (1998)

HST, radio and infrared observations of 28 3CR radio galaxies at redshift $z \sim 1$ – II. Old stellar populations in central cluster galaxies

P. N. Best,[1] M. S. Longair[2] and H. J. A. Röttgering[1]
[1]*Sterrewacht Leiden, Huygens Laboratory, PO Box 9513, 2300 RA Leiden, the Netherlands*
[2]*Cavendish Laboratory, Madingley Road, Cambridge CB3 0HE*

Accepted 1997 October 7. Received 1997 September 29; in original form 1997 March 3

ABSTRACT

Hubble Space Telescope images of 3CR radio galaxies at redshifts $0.6 < z < 1.8$ have shown a remarkable variety of structures, generally aligned along the radio axis, indicating that the radio source strongly influences the optical appearance of these galaxies. In this paper we investigate the host galaxies underlying this aligned emission, combining the *HST* data with ground-based infrared images.

An investigation of the spectral energy distributions of the galaxies shows that the contribution of the aligned blue component to the *K*-band light is generally small (~10 per cent). The radial intensity profiles of the galaxies are well matched at radii $\lesssim$35 kpc by de Vaucouleurs' law, demonstrating that the *K*-band light is dominated by that of an elliptical galaxy. There is no evidence for a nuclear point source, in addition to the de Vaucouleurs profile, with a contribution $\gtrsim$15 per cent of the total *K*-band flux density, except in two cases, 3C 22 and 3C 41. We conclude that the *K*-band emission of the distant 3CR galaxies is dominated by starlight. The magnitudes, colours and location of the distant 3CR galaxies on the projected fundamental plane indicate that their stellar populations formed at high redshift and have since been evolving passively.

Large characteristic radii are derived for the 3CR galaxies, indicating that they must be highly evolved dynamically, even at a redshift of 1. At radii larger than ~35 kpc, a combined galaxy profile clearly shows an excess of emission as compared with de Vaucouleurs' law, indicating that at least some of the galaxies possess cD-type haloes. This supports other independent evidence for the hypothesis that the distant 3CR galaxies lie in moderately rich (proto-)clusters. Since the nearby FR II galaxies in the 3CR catalogue lie in more diffuse environments and do not possess cD haloes, the galactic environments of the 3CR galaxies must change with redshift. The K–z relation of the 3CR galaxies cannot, therefore, be interpreted using a standard 'closed-box, passively evolving stellar population' model, whereby the galaxies that host distant 3CR sources will evolve into the galaxies that host nearby 3CR FR II sources.

At redshifts $z \sim 1$, the absolute *K* magnitudes of the stellar populations of the 3CR galaxies are brighter than those of the lower radio power 6C galaxies, indicating that the 3CR galaxies contain a greater mass of stars; this is consistent with them lying towards the centres of clusters. Powerful high-redshift radio galaxies possess radio beams the kinetic power of which is close to the Eddington limiting luminosity of a central supermassive black hole. Since the mass of the black hole is likely to scale in proportion to the mass of the host galaxy, the 3CR galaxies will contain more massive central engines than the 6C galaxies, which accounts for their more powerful radio emission. At redshifts $z \lesssim 0.6$, the beam power of the radio sources is limited by the availability of fuel for the central engine rather than by the black hole mass, and so no correlation is expected between the radio power and the mass of the host galaxy.

Key words: galaxies: active – galaxies: evolution – galaxies: fundamental parameters – infrared: galaxies – radio continuum: galaxies.

1 INTRODUCTION

The 3CR sample of radio sources defined by Laing et al. (1983) consists of the brightest extragalactic radio sources in the northern sky, selected at 178 MHz, and contains radio galaxies and radio quasars with redshifts up to $z \sim 2$. The host galaxies of the low-redshift sources in the sample are identified with giant elliptical galaxies containing old stellar populations and, if the host galaxies of the high-redshift sources are also giant ellipticals, their stellar populations can be used to study the evolution of this class of galaxy with cosmic epoch and consequently to constrain models of galaxy formation and evolution.

Lilly & Longair (1982, 1984) obtained infrared K magnitudes for an almost complete sample of 83 3CR galaxies with redshifts $0 < z < 1.6$, and constructed the K magnitude versus redshift relation for these objects. The resulting relation showed remarkably little scatter and was interpreted as indicating that the 3CR host galaxies at redshift $z \sim 1$ are indeed giant elliptical galaxies. Lilly & Longair (1984) also showed that, unless the deceleration parameter were as large as $q_0 \sim 3.5$, the shape of the K–z relation would not be consistent with non-evolving stellar populations, but that at least passive evolution is required. The K–z relation suggests that the host galaxies must have formed at large redshift, $z_f \gtrsim 3$; this age is consistent with the red colours of the infrared emission of some of these galaxies (Lilly 1989). Support for such an early formation epoch comes from a very deep spectrum of 3C 65, at redshift $z = 1.176$, which is well-matched using a stellar population of at least 4 Gyr in age (Stockton, Kellogg & Ridgway 1995), and also from the recent results of Dunlop et al. (1996).

In 1987, McCarthy et al. and Chambers, Miley & van Breugel discovered that the optical emission of these powerful radio galaxies tends to be aligned along the axis of the radio source. Many models have been proposed to account for this alignment effect, the most promising being massive star formation induced by the passage of the radio jets (e.g. Rees 1989), scattering of light from an obscured active galactic nucleus (AGN) by electrons or by dust (Cimatti et al. 1996, 1997; Dey & Spinrad 1996, and references therein) and nebular continuum emission from warm line-emitting regions (Dickson et al. 1995). This complicates the use of these galaxies as cosmological probes.

A number of observations have also suggested that a proportion of the K-band light of these galaxies may not be associated with starlight: (i) the discovery of a weaker alignment effect at near-infrared wavelengths (e.g. Eisenhardt & Chokshi 1990; Rigler et al. 1992; Dunlop & Peacock 1993), which may be produced by the long-wavelength tail of a flat-spectrum component responsible for the optical alignment effect; (ii) the detection of broad Hα emission from the distant radio galaxy 3C 22 at $z = 0.938$ (Rawlings et al. 1995; Economou et al. 1995) and a reported detection of an unresolved central component in the K-band emission of 3C 65 at $z = 1.176$ (Lacy et al. 1995), suggesting that the infrared emission may contain light directly from the central AGN; (iii) the observation that infrared emission lines such as [S III] 9532 can contribute a significant percentage of the K-band flux (Rawlings, Eales & Lacy 1991).

In addition, the K–z relation of the 6C radio galaxies, which are roughly a factor of 5 lower in radio luminosity than the 3CR sources, tends to track that of the 3CR galaxies at low redshift, but at higher redshift the 6C galaxies tend to be fainter, lying closer to the 'no evolution' line (Eales & Rawlings 1996; Eales et al. 1997). This result is consistent with the suggestion of Yates, Miller & Peacock (1986) that there is an intrinsic correlation between the absolute infrared magnitude and the radio luminosity of powerful radio galaxies at large redshifts. Eales et al. (1997) have argued that a proportion of the K-band emission of the 3CR galaxies may be directly or indirectly associated with AGN activity, the K–z relation being caused, in part, by the correlation of radio luminosity with redshift in the flux-limited 3CR sample.

In order to study the astrophysics of powerful distant radio galaxies, we have selected an almost complete sample of 28 sources from the 3CR catalogue, in the redshift range $0.6 < z < 1.8$, for observation by the *Hubble Space Telescope* (*HST*). In a previous paper (Best, Longair & Röttgering 1997b; hereafter Paper I) we presented the results of observations of these sources at optical wavelengths using the *HST*, at 8.4 GHz using the Very Large Array radio interferometer (VLA), and at 1.2 and 2.2 μm using the IRCAM3 array on the United Kingdom InfraRed Telescope (UKIRT). The *HST* observations showed that the optical morphologies of the majority of the radio galaxies bear little resemblance to giant elliptical galaxies, being dominated instead by high surface brightness structures elongated along the axes of the double radio sources (Paper I). In interpreting the *HST* images, however, it should be appreciated that standard elliptical galaxies possess very red colours and, at a redshift of 1, have low surface brightnesses at optical (rest-frame ultraviolet) wavelengths (e.g. Giavalisco et al. 1996). Only regions of enhanced ultraviolet emission appear prominently in the images.

We defer an analysis of the variety of optical structures and of the alignment effect to the third paper in this series (Best et al., in preparation, hereafter Paper III). Here, we restrict the investigation to the old stellar populations of the host radio galaxies. The outline of this paper is as follows. In Section 2, we describe the data reduction used in the current analysis that has not already been discussed in Paper I. In Section 3, we address the problem of estimating the fraction of the K-band light that is associated with a flat-spectrum aligned component. In Section 4 we investigate the radial intensity profiles of the galaxies. The relationship between the half-light radii and the surface brightnesses of the galaxies is compared with the locus of low-redshift elliptical galaxies and brightest cluster galaxies in Section 5. In Section 6 we derive an improved K–z relation for the narrow-line radio galaxies. The implications of our results for the formation and evolution of massive galaxies and for the cosmic evolution of the radio source population are discussed in Section 7, and we summarize our conclusions in Section 8.

Throughout the paper, the GISSEL stellar synthesis codes of Bruzual & Charlot (1993) are used. We adopt a Scalo (1986) initial mass function with upper and lower mass cut-offs of 65 and 0.1 $M_\odot$ respectively, and solar metallicity. Except where otherwise stated, a deceleration parameter $q_0 = 0.5$ and a Hubble constant $H_0 = 50\,\mathrm{km\,s^{-1}\,Mpc^{-1}}$ are adopted.

2 THE DATA

A variety of infrared properties of the galaxies were measured directly from the infrared images and are presented in Table 1 (see also the data tables presented in Paper I). Table 2 contains properties of the galaxies that are derived in the text.

The photometric magnitudes of the galaxies were measured at a variety of wavelengths (see Paper I), and were converted into broad-band flux densities for the investigation of the spectral energy distributions (SEDs) of the galaxies in Section 3. Most of the optical flux densities are influenced to some extent by emission lines that lie

Table 1. Measured properties of the radio galaxies (see Paper I).

Source	z	K-mag. [9″ diam. ap.]	Error	Ellip.	D.P.A. [deg]	K_{corr}
(1)	(2)	(3)	(4)	(5)	(6)	(7)
3C 13	1.351	17.52*	0.06	0.12	12	17.43
3C 22	0.938	15.40	0.15	0.12	12	–
3C 34	0.690	16.43*	0.05	0.10	29	16.15
3C 41	0.795	15.68	0.04	0.21	54	–
3C 49	0.621	16.15	0.15	0.20	8	16.22
3C 65	1.176	16.59	0.07	0.16	60	16.60
3C 68.2	1.575	17.49	0.12	0.28	4	17.66
3C 217	0.897	17.52	0.08	0.22	51	17.67
3C 226	0.820	16.52	0.05	0.12	76	16.73
3C 239	1.781	17.83*	0.06	0.07	80	17.70
3C 241	1.617	17.45	0.08	0.18	26	17.51
3C 247	0.749	15.96*	0.10	0.08	25	15.78
3C 252	1.105	17.32	0.07	0.22	1	17.69
3C 265	0.811	16.03	0.04	0.12	14	16.26
3C 266	1.272	17.88*	0.09	0.10	3	17.95
3C 267	1.144	17.21	0.05	0.36	38	17.33
3C 277.2	0.766	17.27*	0.05	0.11	22	17.33
3C 280	0.996	16.99*	0.04	0.10	68	16.85
3C 289	0.967	16.66	0.07	0.19	65	16.71
3C 324	1.207	16.99	0.06	0.24	8	17.11
3C 337	0.635	16.57	0.08	0.13	6	16.60
3C 340	0.775	16.91	0.08	0.14	16	16.98
3C 352	0.806	16.92*	0.05	0.13	35	16.81
3C 356	1.079	17.50*	0.06	0.06	15	17.41
3C 368	1.132	17.03**	0.15	0.32	3	17.34
3C 437	1.480	17.74	0.20	0.11	77	17.74
3C 441	0.708	16.42*	0.04	0.02	0	16.26
3C 470	1.653	18.02*	0.15	0.32	83	17.77

Column 1 contains the 3C catalogue name of the source, with its redshift in column 2. The K magnitude measured from our UKIRT images is given in column 3, with the error in column 4. This was generally measured through a 9-arcsec aperture (for those galaxies indicated by an asterisk, a 5 arcsec diameter aperture was used to exclude nearby companions; see Paper I), and has been corrected for galactic extinction using the extinction maps of Burstein & Heiles (1982). For 3C 368 (marked **) the K magnitude quoted is after subtraction of the M star (see Paper I). The ellipticity of the K-band image is given in column 5 and the position angle offset from the radio axis in column 6. In column 7 we tabulate the K_{corr} magnitudes obtained after scaling to a 9 arcsec diameter aperture and correcting for any flat-spectrum and point-source contributions (see text).

within the passband of the filter. In Paper I, we calculated the percentage of the flux density that is associated with line emission for each of the *HST* observations; these values are used to produce 'true' broad-band continuum flux densities. In addition, the contributions of the [O III] 4959, 5007 and Hβ emission lines to the J-band flux densities of those galaxies at redshifts $z \gtrsim 1.1$ have been estimated from the [O II] 3727 line flux, using line ratios taken from the combined radio galaxy spectrum derived by McCarthy (1993), and have been subtracted from the J-band magnitudes. No correction has been made for line contamination in the K waveband, although this should produce little error since strong lines such as Hα do not enter the K waveband until a redshift of $z \sim 1.9$, which is greater than that of any of the sources in the sample. The only emission line of any significance that may be present in the K band is the [S III] 9532 line. Rawlings et al. (1991) detected a significant (~15 per cent) contribution to the K-band flux density of 3C 356 in this line, but in none of the other galaxies that they observed was its contribution greater than ~5 to 10 per cent, and often the line was not detected. In addition, this line only falls in the K band for the eight galaxies with redshifts $1.05 < z < 1.55$, and these galaxies do not have significantly brighter absolute K magnitudes.

Another factor that influences the measured flux densities is reddening by dust intrinsic to the galaxies. Since no accurate estimates have yet been made of the mass, temperature and distribution of dust throughout these galaxies, taking account of dust extinction is problematic. It has a negligible effect at the long wavelengths of the K-band emission, with which most of this paper is concerned, but it will affect the SED fitting in Section 3.1.

The distribution of dust within elliptical galaxies can be divided into two components. First, there is dust spread throughout the galaxies: this affects the colours of the galaxies but has little effect upon their morphologies. This dust is therefore impossible to detect in our observations, and cannot be properly compensated for. We discuss this extended dust briefly when modelling the SED in

Table 2. Properties of the radio galaxies derived in the various sections of the paper.

Source	Stellar Mass	Flat Spec. Flux	Flat Spec. (K-band)	Align. Str. (K-band)	r_e	% Point Source	% Point Source	Point Source Limits	μ_e K-band	μ_e V-band (passive)
	$[10^{11}\,M_\odot]$	[μJy]	[%]		["]	[Measured]	[Corrected]		[Mags per sq. arcsec]	
(1)	(2)	(3)	(4)	(5)	(6)	(7)	(8)	(9)	(10)	(11)
3C 13	5.5	9.0	15	0.09	1.25	0	0	$P < 7$	19.91	22.31
3C 22	–	–	–	0.09	1.5	37	50	$40 < P < 70$	–	–
3C 34	4.2	2.0	2	0.04	3.9	5	5	$P < 11$	21.10	23.96
3C 41	–	–	–	−0.04	2.3	24	31	$23 < P < 41$	–	–
3C 49	4.5	8.5	7	0.16	1.05	0	0	$P < 2$	18.32	21.24
3C 65	8.5	1.5	1	−0.05	1.7	0	0	$P < 8$	19.75	22.32
3C 68.2	5.5	8.0	17	0.26	–	–	–	–	–	–
3C 217	2.6	9.0	17	−0.03	2.3	0	0	$P < 6$	21.47	24.24
3C 226	5.7	7.0	6	−0.08	2.55	7	13	$P < 21$	20.75	23.55
3C 239	5.8	8.0	19	−0.05	–	–	–	–	–	–
3C 241	7.7	3.5	6	0.08	–	–	–	–	–	–
3C 247	7.5	3.2	2	0.04	–	–	–	–	–	–
3C 252	3.1	12.0	23	0.22	1.4	8	17	$P < 24$	20.41	23.06
3C 265	10.0	35.0	16	0.08	1.9	4	8	$P < 12$	19.65	22.45
3C 266	3.2	11.0	24	0.10	1.5	2	4	$P < 13$	20.83	23.33
3C 267	4.5	7.5	12	0.06	1.7	0	0	$P < 5$	20.48	23.10
3C 277.2	3.5	8.0	10	0.06	2.0	8	15	$P < 21$	20.83	23.64
3C 280	6.7	9.5	9	−0.05	1.15	0	0	$P < 8$	19.14	21.85
3C 289	6.5	4.5	4	−0.08	2.45	1	1	$P < 7$	20.65	23.38
3C 324	5.0	8.0	12	0.20	2.2	0	0	$P < 4$	20.81	23.38
3C 337	3.5	1.2	1	0.11	1.15	2	2	$P < 9$	18.90	21.81
3C 340	3.5	5.0	7	0.09	0.7	0	0	$P < 4$	18.20	21.02
3C 352	3.7	5.0	7	0.03	2.0	4	7	$P < 13$	20.31	23.11
3C 356	2.7	7.0	16	0.04	0.9	0	0	$P < 14$	19.17	21.84
3C 368	3.6	21.0	31	0.30	–	–	–	–	–	–
3C 437	4.2*	3.5*	–	−0.08	–	–	–	–	–	–
3C 441	5.0	4.0	4	0.02	1.65	0	0	$P < 5$	19.35	22.24
3C 470	4.0*	2.7*	–	−0.27	–	–	–	–	–	–

Column 1 contains the 3C catalogue name of the source. Column 2 lists the stellar mass of the galaxy derived from the fits in Section 3.1, and column 3 the flux density at rest-frame 3000 Å of the 'flat spectrum' component derived from the same fit. The values for 3C 437 and 3C 470 (marked with an asterisk) are only estimates since only two broad-band flux densities were available. This analysis was not possible for 3C 22 and 3C 41 because of a nuclear contribution to their flux densities. For the remaining 24 galaxies, the approximate percentage of the K-band light that is associated with a flat-spectrum aligned component is given in column 4. The K-band alignment strength of each galaxy, as defined in Section 3.2, is listed in column 5. Column 6 gives the best-fitting de Vaucouleurs radius for each galaxy (see Section 4, where the errors involved are also discussed). Such fits were not possible for 3C 247 and 3C 368, nor for the five highest redshift sources (see text). The percentage of K-band light associated with an unresolved nuclear emission source in the best-fitting model is given in column 7. The value after a correction factor has been applied (see Section 4 for further details) is given in column 8, and the 90 per cent confidence limits for this value are given in column 9. The measured mean surface brightness within the de Vaucouleurs radius in the K band is given in column 10, and the modelled V-band surface brightness for a passive-evolution model is listed in column 11 (see Section 5 for more details). This analysis was not carried out for 3C 22 and 3C 41 because of the presence of a nuclear contribution to the K-band flux.

Section 3.1. The second dust component is that which lies in discs near the centres of the galaxies; de Koff et al. (1996) showed that between 30 and 40 per cent of low-redshift radio galaxies possess clear dust lanes. The most prominent example of this phenomenon in the galaxies in our sample is the large dust lane running across the central regions of 3C 324. Dickinson, Dey & Spinrad (1996) showed that an extinction $E(B-V) \sim 0.3$ is required in the central regions of this galaxy to obscure the galaxy nucleus; at the wavelengths of the *HST* observations, this extinction coefficient corresponds to removing about 70 per cent of the flux density from the regions underlying the dust lane (e.g. de Vaucouleurs & Buta 1983). For 3C 324, this correction results in a 19 per cent increase in the total flux density through the F702W filter, and 16 per cent through the F791W filter.

Four other galaxies, 3C 68.2, 3C 252, 3C 266 and 3C 356, also show reasonably convincing evidence for dust lanes, although not to the extent of 3C 324.[1] The much more compact dust lanes in these sources, relative to that of 3C 324, make accurate measurements of the extinction coefficient impractical, and so we adopt a value of half of that of 3C 324. Repeating the above procedure for these galaxies provides best estimates of the optical flux density corrections of, in order of increasing wavelength for each source: 3C 68.2, 7 per cent; 3C 252, 7, 4 per cent; 3C 266, 10, 5, 4 per cent; 3C 356, 6,

[1]Note that there is marginal evidence for weaker dust lanes in the central regions of other galaxies in the sample; however, these are too weak for reliable estimates of their effect to be made and, in any case, the increase in flux density would be ≲5 per cent. de Koff et al. (1996) suggested that the frequency of dust lanes in the 3CR radio galaxies with redshifts $0.1 < z < 0.5$ is invariant with redshift, corresponding to about 30 to 40 per cent of all the sources. Our images would be consistent with a similar percentage of dust lanes being present in the high-redshift 3CR galaxies.

4 per cent. These corrections have been incorporated into the flux density measurements used in the next section.

3 THE INFRARED ALIGNED COMPONENT

3.1 Fits to the spectral energy distributions

The infrared observations presented in Paper I confirm the result that the *K*-band emission of the powerful radio galaxies in our sample has a tendency to be aligned along the radio axis (Eisenhardt & Chokshi 1990; Rigler et al. 1992; Dunlop & Peacock 1993) but it is a significantly weaker effect than in the optical waveband. This aligned infrared emission may be the long-wavelength tail of the flat-spectrum component responsible for the alignment effect in the optical waveband, or may indicate that the old stellar population itself is aligned with the radio source, as in the models of Eales (1992) and West (1991, 1994).

A relatively simple procedure has been adopted for estimating the contribution of the optically aligned component to the infrared alignment. For each galaxy an SED is produced that best matches the observed broad-band flux densities, using the sum of two components. The first component is an old stellar population, the SED of which is derived using the GISSEL stellar synthesis codes of Bruzual & Charlot (1993). We assume that the stars formed in a 1-Gyr burst which occurred at redshift $z = 10$, and the stellar population then evolved passively until the observed epoch; negligible changes result for the SED at redshift $z \sim 1$ if a formation redshift of 5 or 50, or an exponentially decreasing star formation rate is used instead. The second component represents the aligned emission; the spectral shape of this component depends upon the physical cause of the alignment effect.

For electron scattering, a power-law quasar spectrum is expected, $f_\nu \propto \nu^\alpha$, where the value of α is generally about -0.7 to -1 for quasars (e.g. Baker & Hunstead 1996). Owing to the much lower scattering efficiency of electrons compared with dust (e.g. di Serego Alighieri, Cimatti & Fosbury 1994), if electron scattering is to dominate, then the mass of extended dust must be small, and extinction by the extended dust will have little effect on the spectral shape. If scattering by dust is entirely responsible for the excess ultraviolet flux then, assuming the dust to be evenly distributed throughout the galaxies, a few times $10^7\,M_\odot$ of dust are required (e.g. di Serego Alighieri et al. 1994). Light scattered by this dust will have a spectrum somewhat bluer than the incident quasar power law (Calzetti et al. 1995; Cimatti et al. 1996), but dust outside the scattering regions will redden the scattered emission, giving it a similar spectral shape to electron scattering. A young starburst has a spectral shape which is relatively flat in f_ν, whilst nebular continuum emission has a much redder spectrum below about rest-frame 3600 Å but provides little *K*-band intensity. Each of these effects is likely to be present at some level, and so the overall SED of the aligned component will be some combination of these. For illustrative purposes, we will assume that one-third of the aligned emission at rest-frame 3600 Å is associated with each of the three processes of scattering, star formation and nebular continuum; this is well within the range of previous estimates (e.g. Dickson et al. 1995; Cimatti et al. 1997; Tadhunter, Dickson & Shaw 1996). This combination can be approximated from optical wavelengths through to the *K* band by a single spectral shape, $f_\nu \propto \nu^{-0.4}$, which is in close agreement with the $f_\nu \propto \nu^{-0.2}$ rest-frame ultraviolet spectral shape determined for the powerful radio galaxy 4C41.17 (Dey et al. 1997). This, $f_\nu \propto \nu^{-0.4}$, is the spectral shape we adopt for the aligned emission, and hereafter we refer to this component as the 'flat-spectrum component'.

For each galaxy, the old stellar population and flat-spectrum components were weighted to produce the combined spectrum that best matched the broad-band flux densities measured in the UKIRT and *HST* observations. These fits are shown in Fig. 1. Such fits were not made for 3C 437 and 3C 470, for which only two broad-band flux densities were available, nor for 3C 22 and 3C 41 which both possess significant nuclear components in the infrared images (see Section 4).

The fits shown in Fig. 1 are, in the majority of cases, rather good, indicating that the simple two-component model of the SED can provide a good representation of the spectra of these galaxies. The mass of stars within the galaxy and the flux density of the flat-spectrum component are listed in Table 2. Notice that the stellar masses are typically a few times $10^{11}\,M_\odot$ which, given that the mass-to-light ratios of such galaxies are usually well in excess of 1, demonstrates that these galaxies are significantly more massive than M^*. The contributions to the *K*-band flux of the two components of the fit can be compared to provide an estimate of the fraction of the emission in this band that is associated with the aligned component. The values derived from our best-fitting models are tabulated in Table 2 and range from ~1 per cent in the passive sources 3C 65 and 3C 337, up to ~31 per cent in the case of 3C 368, with an mean value of about 10 per cent.

3.2 The origin of the aligned infrared emission

To quantify the degree of alignment, we define the *alignment strength* as

$$a_s = \epsilon\left(1 - \frac{\Delta\theta}{45}\right),$$

where $\Delta\theta$ is the difference in position angle between the *K*-band emission and the radio axis, measured in degrees, and ϵ is the ellipticity of the *K*-band image, defined as

$$\epsilon = \left[1 - \left(\overline{q^2}/\overline{p^2}\right)\right]^{1/2},$$

where p and q are dimensions along the major and minor axes respectively of the infrared image of the radio galaxy. The alignment strength therefore ranges from +1 to −1: those galaxies in which the major axis of the infrared emission is oriented within 45° of the radio axis have a positive alignment strength, whilst those that are misaligned have a negative value; a value of zero corresponds either to a galaxy with a major axis that is misaligned by 45° from the radio axis, or to a galaxy that is circularly symmetric. This is a better statistic than considering $\Delta\theta$ alone since it results in a higher value for a source that is highly elongated but misaligned by, say, 15° from the axis of the radio emission than for a source that is virtually symmetric but with a major axis lying directly along the radio axis. The values of the *K*-band alignment strengths are tabulated in Table 2 and are plotted as a histogram in Fig. 2. There is a clear tendency for the galaxies to show some alignment in the *K* waveband, with nearly 70 per cent possessing positive alignment strengths, a result significant at greater than the 95 per cent confidence level. The mean value of the alignment strength is 0.05.

It is interesting to compare the *K*-band alignment strength with the percentage flat-spectrum contribution in the *K* band (Fig. 3). Of the five galaxies with the largest *K*-band flat-spectrum components, four are amongst the seven sources with high *K*-band alignment strengths, $a_s \geq 0.10$, including all three in the highest bin in Fig. 2

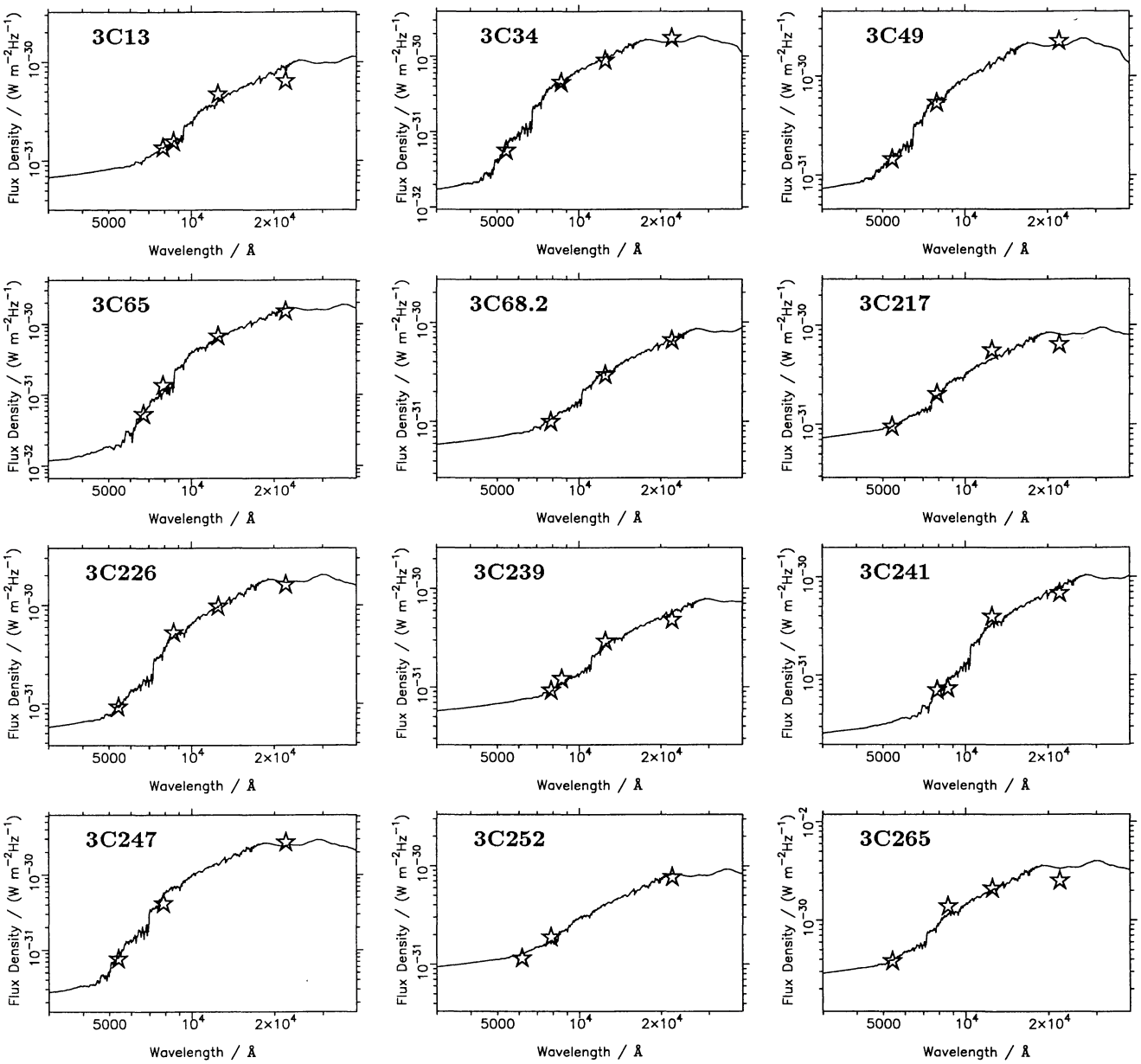

Figure 1. SED fits to the broad-band flux densities of the 3CR galaxies using an old stellar population and an aligned component (see text and Table 2 for details).

(see also Table 2). A Spearmann rank test indicates that these parameters are correlated, at a significance level of about 97.5 per cent. If the four sources, 3C 68.2, 3C 252, 3C 266 and 3C 368, with particularly high values of both a_s and the flat-spectrum contribution are excluded, then for the remaining 24 galaxies the average alignment strength is $\langle a_s \rangle = 0.02$, different from the hypothesis of no alignment at only low significance.

The correlation displayed in Fig. 3 indicates that the long-wavelength tail of the active blue emission responsible for the alignment of the optical images is an important source of the *K*-band alignment effect. Scatter in this relation will arise from the errors introduced in determining the two parameters from the data and, more importantly, from any intrinsic scatter in the alignment strength, such as that suggested by the negative tail in Fig. 2. An estimate of the underlying scatter can be gauged from the range of alignment strengths in Fig. 3 of those galaxies with only small flat-spectrum components, suggesting a standard deviation of between 0.05 and 0.1. If the parent galaxies are giant elliptical galaxies, this can naturally be explained in terms of the radio axis being randomly orientated with respect to the major axis of the galaxy.

4 RADIAL LIGHT PROFILES

Our observations can be used to test whether the *K*-band light distributions of the galaxies have the profiles of elliptical galaxies, by attempting to fit de Vaucouleurs' law, $I(r) \propto \exp[-7.67(r/r_e)^{1/4}]$, to their radial surface brightness profiles. The *HST* images allow such plots to be made without the need to account for the effects of seeing, and would allow an excellent determination of the radial profiles to be made, were it not for the fact that at optical wavelengths the emission from the majority of

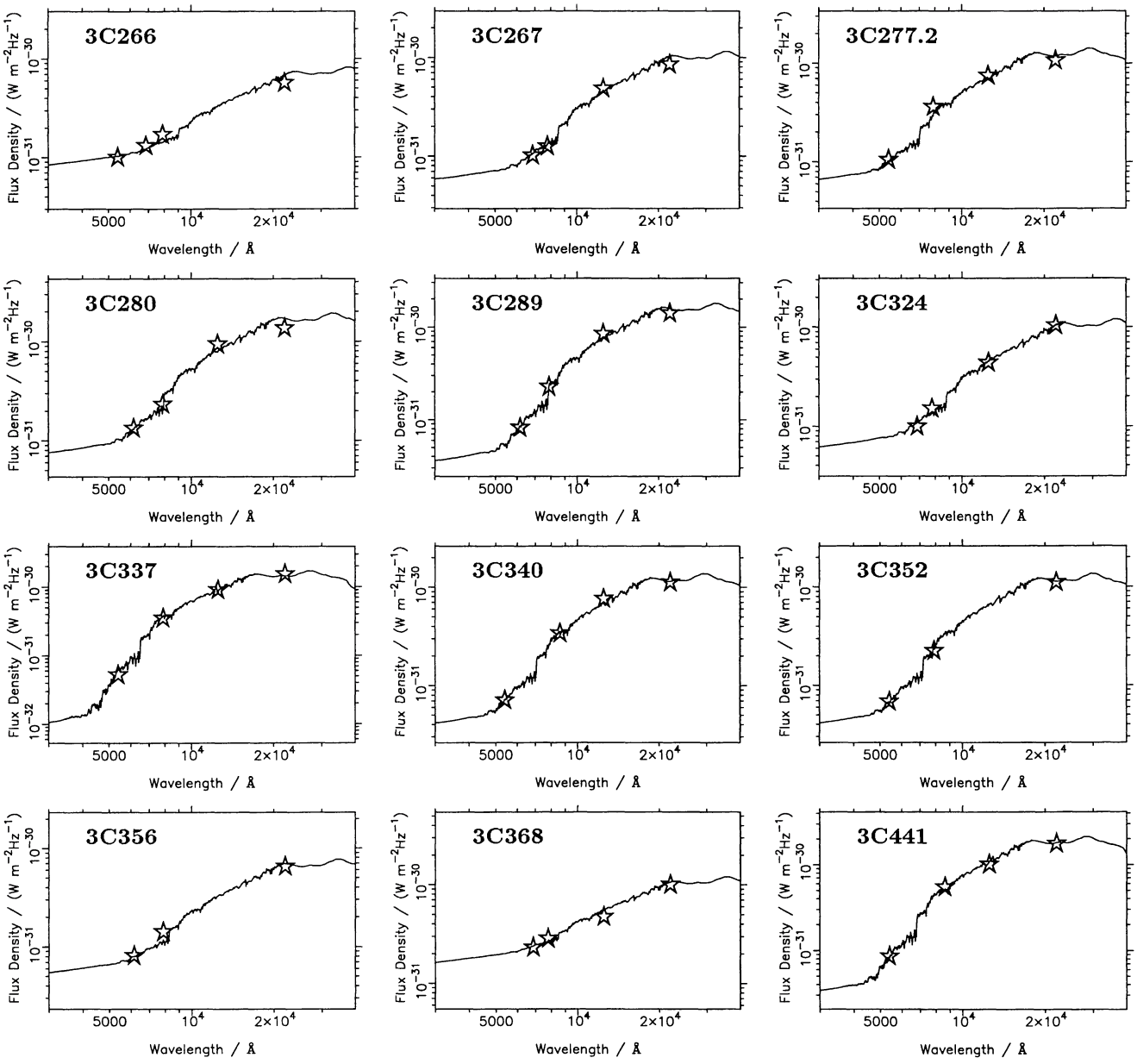

Figure 1 – *continued*

the galaxies is dominated by the aligned blue component and so this analysis cannot be carried out. Eight of the galaxies, however, do not show strong ultraviolet emission. The *HST* images show that they possess almost symmetrical morphologies, and only weak aligned components are required to fit their SEDs ($\lesssim$10 per cent of the total flux density in the *HST* image). The radial intensity profiles of the optical emission of these galaxies were measured, nearby companion objects being removed and replaced with the average background intensity at that distance from the centre of the galaxy. No companion subtended an angle greater than 20° about the centre of the galaxy, and so any errors in this replacement will be small. The radial profiles are displayed in Fig. 4. They show that a de Vaucouleurs profile provides an excellent fit to the observed radial surface brightness in six of the eight cases, providing some of the strongest evidence to date that these high-redshift galaxies are indeed giant elliptical galaxies. The derived values of r_e are listed

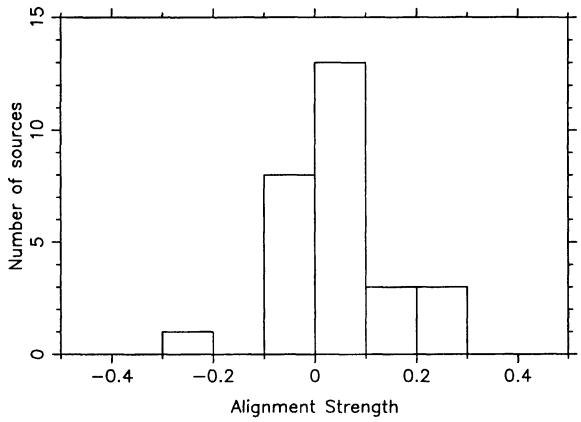

Figure 2. A histogram of the *K*-band alignment strengths. Values lying on a boundary are included in the lower bin.

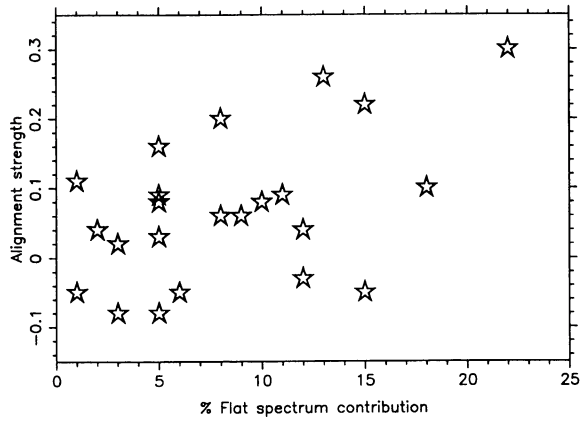

Figure 3. A plot of the *K*-band alignment strength against the percentage contribution at *K* of the flat-spectrum component required to match the SED of the galaxy.

in Table 2, and have a typical accuracy of about 15 per cent. The cases of 3C 22 and 3C 41, the two sources for which a good de Vaucouleurs fit is not obtained at small radii, are discussed below.

The characteristic radii, r_e, obtained from these fits were then used to investigate the infrared *K*-band radial intensity profiles. Where companion galaxies subtended less than about 45° with respect to the centre of the galaxy, these were removed as in the *HST* images, and replaced by the average of the background pixels at that point. In two cases, 3C 34 and 3C 441, nearby companion galaxies subtended an angle $\gtrsim$45° about the centre of the 3CR galaxy, and this substitution could lead to large errors in the radial profiles. In these cases, the radial intensity profile out to a radius of about 1 arcsec was determined using the normal method, but at larger radii only the two or three quadrants around the source that did not contain the companion were used, and the emission from these was then scaled to derive the average intensities. The two methods matched well at the boundary at 1-arcsec radius.

The infrared radial intensity profiles of these eight galaxies were modelled using a two-component fit, involving a de Vaucouleurs profile with the characteristic radius determined from the fits to the *HST* images, and a point source of emission; each profile was convolved with a Gaussian profile matching the seeing of the infrared observations. The seeing, which was typically between 1 and 1.2 arcsec, was measured using objects on the infrared images of the radio galaxy that appeared unresolved in the *HST* data. The fitting procedure involved minimizing the sum of the squares of the offsets of the combined model profile from the data points within the inner 3-arcsec radius, weighting each data point inversely by its error. Tests showed that the procedure converged to the same minima from a complete range of initial values.

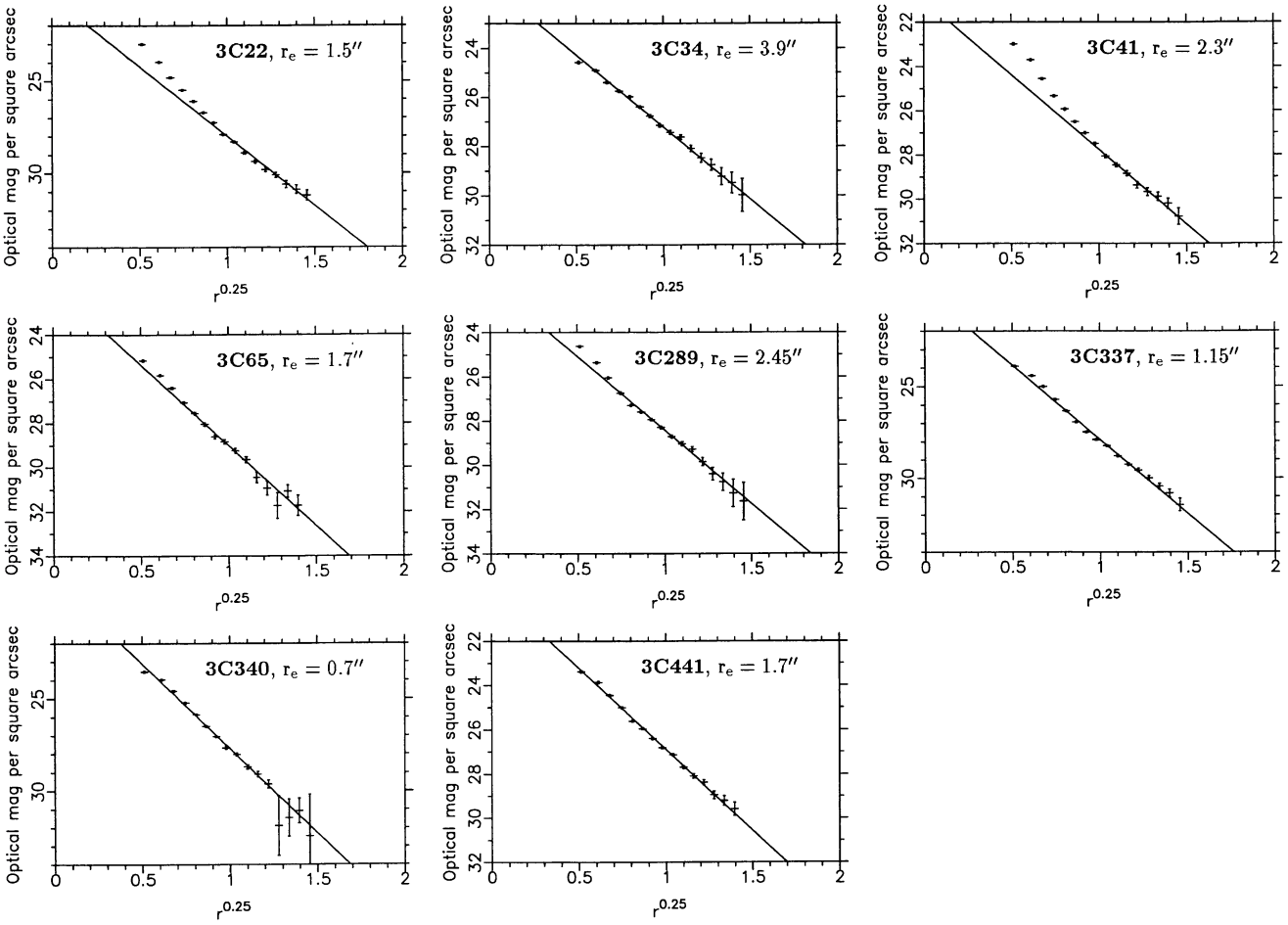

Figure 4. de Vaucouleurs fits to the radial intensity profiles of the *HST* images of eight 3CR radio galaxies which do not show a significant active ultraviolet component. The characteristic radius of each, determined from the gradient of the best-fitting straight line, is given.

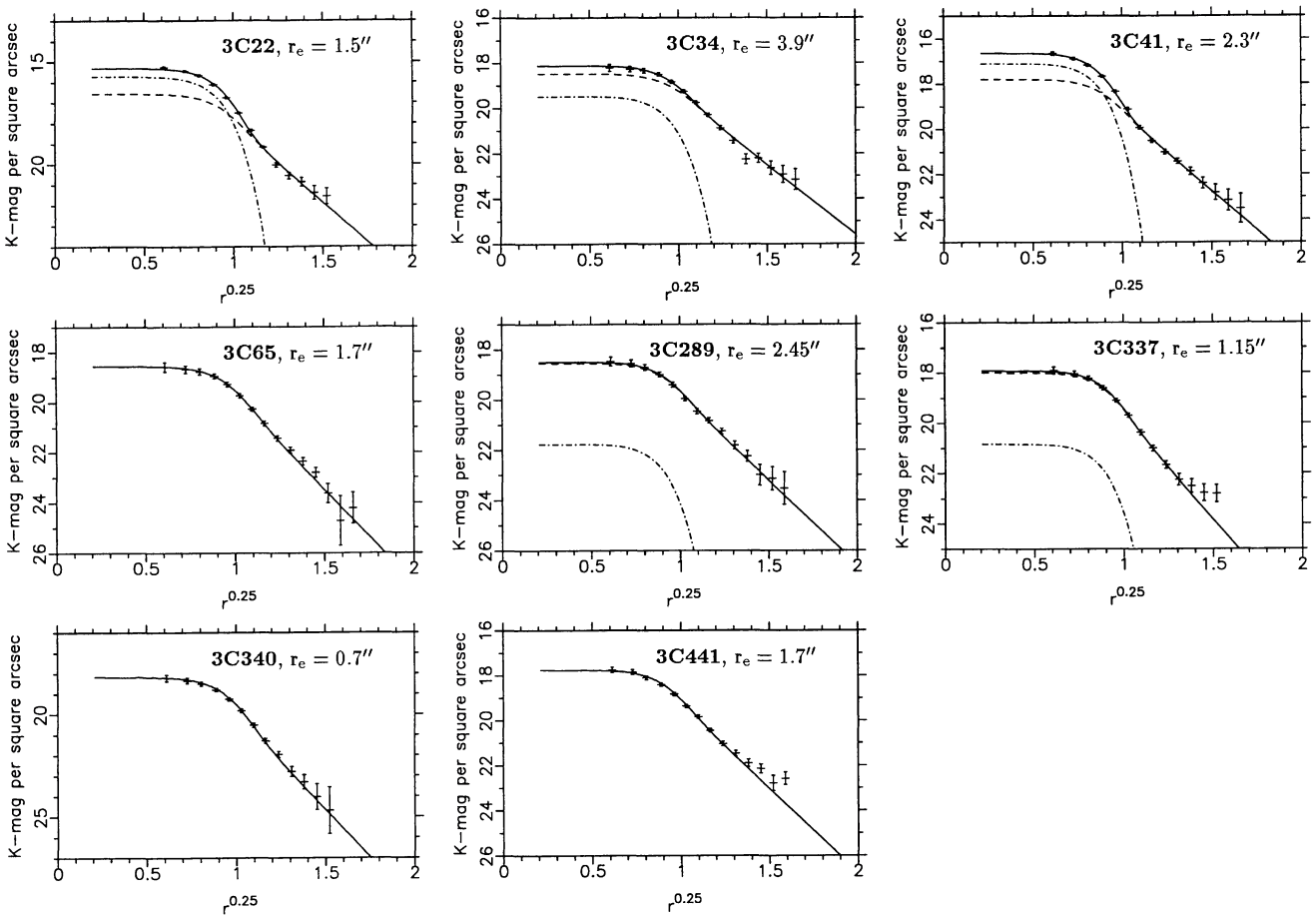

Figure 5. Fits to the radial intensity profiles of the *K*-band images of the eight 3CR galaxies shown in Fig. 4, using the sum of an unresolved point source (dash–dotted line) and a de Vaucouleurs profile with the characteristic radius determined from the *HST* images (dashed line). For each of the profiles, the effect of seeing has been taken into account. The sum of the two components is indicated by the solid line. In many cases the best fit does not involve a point-source component, and so only the solid line is shown.

The resulting fits are shown in Fig. 5: the dashed line shows the de Vaucouleurs profile, the dash–dotted line shows the radial profile of the point source, and the solid line shows the total intensity profile. In several cases, the point-source component is zero, and so only the solid line is plotted. In each case a good match is obtained. The percentage of the total *K*-band emission of each source associated with a point source for the best-fitting combination is given in Table 2.

This analysis indicates the reason for the poorness of fit of the de Vaucouleurs profiles to the optical radial intensity profiles of 3C 22 and 3C 41: the fits for these galaxies indicate the presence of an unresolved nuclear component contributing 37 and 24 per cent of the total *K*-band flux respectively. It is interesting that these galaxies are the most luminous in our sample in the *K* band, lying furthest from the mean K–z relation. Rawlings et al. (1995) have already suggested that 3C 22 is a reddened quasar observed close to the radio galaxy/quasar divide, based upon the compactness of the infrared emission, the detection of broad Hα emission in their spectrum and that of Economou et al. (1995), and the very red colour of its spectral energy distribution. This hypothesis is supported by the fact that this source possesses a bright radio core and a strong one-sided jet, features which are characteristic of quasars, but not generally of radio galaxies (see Paper I for further discussion). No such claim has yet been made for 3C 41, although we note that it is one of the few sources in the sample to possess a clear radio jet (Paper I).

Table 3. The percentage of point-source component determined by the fitting routine for a given percentage of star added to the radio galaxy. This was carried out for fitting both when the characteristic radius was known from the *HST* data, and when it was a free parameter in the fit.

% star added	% point source recovered	
	Known r_e	Variable r_e
5	4.5 ± 1.3	2.8 ± 1.5
10	8.8 ± 1.4	4.8 ± 2.2
15	12.9 ± 1.5	6.9 ± 2.4
20	16.4 ± 1.8	9.0 ± 2.9
25	20.0 ± 2.1	11.9 ± 3.1
30	23.6 ± 2.4	13.4 ± 2.7
40	30.6 ± 2.9	20.8 ± 2.9
50	37.5 ± 3.4	26.8 ± 3.0
60	44.5 ± 3.5	32.3 ± 3.5

Given the small size of these galaxies relative to the seeing profile, to test the accuracy of the fitting procedure for determining the nuclear point source contribution, we added the emission from a star, at various percentages of the total flux density, to the infrared

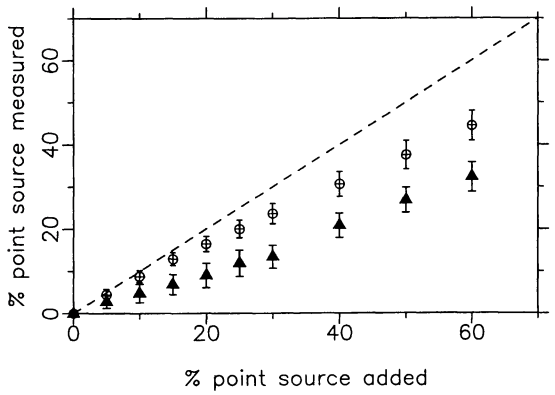

Figure 6. The percentage of point-source component determined by the fitting routine for a given percentage of star added to the radio galaxy. The crossed circles show the results when the characteristic radius was known from the *HST* data, and the filled triangles show the corresponding values for the galaxies for which the characteristic radius was a free parameter in the fit.

images of a number of the radio galaxies. The resultant images were passed through our fitting procedure to determine the percentage nuclear point source recovered. The results are given in Table 3 and plotted in Fig. 6 (crossed circles). For additions of a star of up to about 15 per cent of the total flux density, the recovery of the point-source component is almost total, giving confidence to the result that there is little or no requirement for a nuclear contribution in six of the galaxies in Fig. 5. In particular, there is no evidence, either in the de Vaucouleurs fit or in the SED, for the strong (~45 per cent) nuclear contribution to the emission of 3C 65 suggested by Lacy et al. (1995). For larger levels of star added, typically only about 75 per cent of the flux density is recovered as a point-source. These results suggest that the true point-source contribution for 3C 41 will be approximately 30 per cent, and for 3C 22 the best-fitting value will be about 50 per cent, with an upper limit of as much as about 70 per cent of the emission being associated with an unresolved nuclear component. The 'corrected' point-source contributions are given in Table 2, together with the 90 per cent confidence limits to this value as determined from the least-squares fits.

Radial intensity profile fits can also be made for those galaxies that possess enhanced ultraviolet emission in the *HST* images, since these too are dominated by the underlying old stellar population at infrared wavelengths. 3C 368 and 3C 247 were omitted from this analysis, the former because of the presence of a foreground star within the galaxy envelope which cannot be accurately removed (see Paper I), and the latter because it is surrounded by nearby companions, too many to employ the quadrant method discussed above. The five highest redshift galaxies in the sample were also omitted owing to low signal-to-noise ratios of the infrared emission at large radii.

For the remaining 13 galaxies the infrared radial intensity profiles were measured, and the best-fitting matches were derived from the sum of an unresolved point source and a de Vaucouleurs profile. The characteristic radius of the de Vaucouleurs profile was allowed to vary to obtain the best match. The best-fitting models are compared with the observations in Fig. 7, with the same notation as in Fig. 5, and the parameters of the models are given in Table 2. Although the individual values of r_e can only be determined to a typical accuracy of about 35 per cent, the galaxy light profiles can again be well fitted using this model.

The small size of the galaxies leads to some degeneracy between the characteristic radius and the point source contribution. We have repeated the test of adding a point source to the radio galaxies, allowing the characteristic radius r_e to vary in the fit. The results are given in Table 3 and shown in Fig. 6. The contribution of point source measured was lower than was added throughout, typically by about a factor of 2. What is happening is that the fitting routine is estimating a slightly smaller value for r_e, and attributing the remainder of the point-source flux to the galaxy profile. The error on the points in Fig. 6 represents the scatter in the results for addition to different galaxies, and arises predominantly from the range of characteristic radii in the sample: the recovery of the point source is least effective for those sources with the smallest characteristic radii. However, even for small additions of a stellar component, some point-source contribution was generally recovered, and therefore the very low point-source percentages required for the galaxies in Fig. 7 (mean value $\lesssim$4 per cent) give confidence that any nuclear contribution must be small. The 'corrected' contributions of the unresolved emission to the *K*-band flux density are listed in Table 2 together with the 90 per cent confidence limits on these values. Each of these galaxies is consistent with no point-source component being present.

For a significant fraction of the galaxies, the observed profiles become brighter than the predicted de Vaucouleurs profile at large radii, suggesting that at least some of these galaxies possess diffuse extended envelopes. The reality of these envelopes for any individual galaxy cannot be gauged because the signal-to-noise ratio of this extended emission is low and, more importantly, the errors at large radii are dominated by uncertainties in the background subtraction and so are not necessarily independent. We have therefore combined the radial intensity profiles of the galaxies. The radial profile of each galaxy was scaled to the same characteristic radius, enabling the galaxy profiles to be summed directly. Only those galaxies for which $1.0 \leq r_e \leq 2.0$ were included: for galaxies with a smaller r_e there remains a significant contribution owing to the seeing at radii of 2 to 3 r_e, whilst for galaxies with r_e greater than 2, there is insufficient signal at the largest radii to test for the presence of the halo. The scaled radial profiles of the remaining 12 galaxies were summed, weighting each galaxy equally, and the results are presented in Fig. 8.

At radii greater than about 2.4 r_e, that is, $(r/r_e)^{1/4} \sim 1.25$, at which the effects of seeing should be small, a significant halo component has been detected. This envelope extends from a physical radius of typically about 35 kpc out to at least 60 kpc, and probably further. This extended envelope may be dominated by the emission from only a small number of the radio galaxies, but it must be present in at least some of them.

The halo emission is not an artefact associated with the flat-spectrum contribution to the *K*-band emission, for two reasons. First, on the *HST* images (Paper I), well over 95 per cent of the flat-spectrum emission originates at radii less than 35 kpc, the radius at which evidence for the halo component first appears; secondly, if the 12 galaxies are split into two groups according to the percentage of flat-spectrum light in the *K*-band image, there is no significant difference between the strengths of the halo component in the two samples. We have also studied the profiles of stars of the images to check that this halo is not an artefact associated with wings in the UKIRT point spread function.

Such a halo component is typical of cD galaxies (e.g. Oemler 1976). Thuan & Rominishin (1981) compared the radial intensity profiles of brightest cluster galaxies in rich and poor clusters of galaxies, and showed that enhanced halo components were only seen around the central galaxies of rich clusters, and that they begin at radii between about 25 and 40 kpc, comparable to the 35 kpc

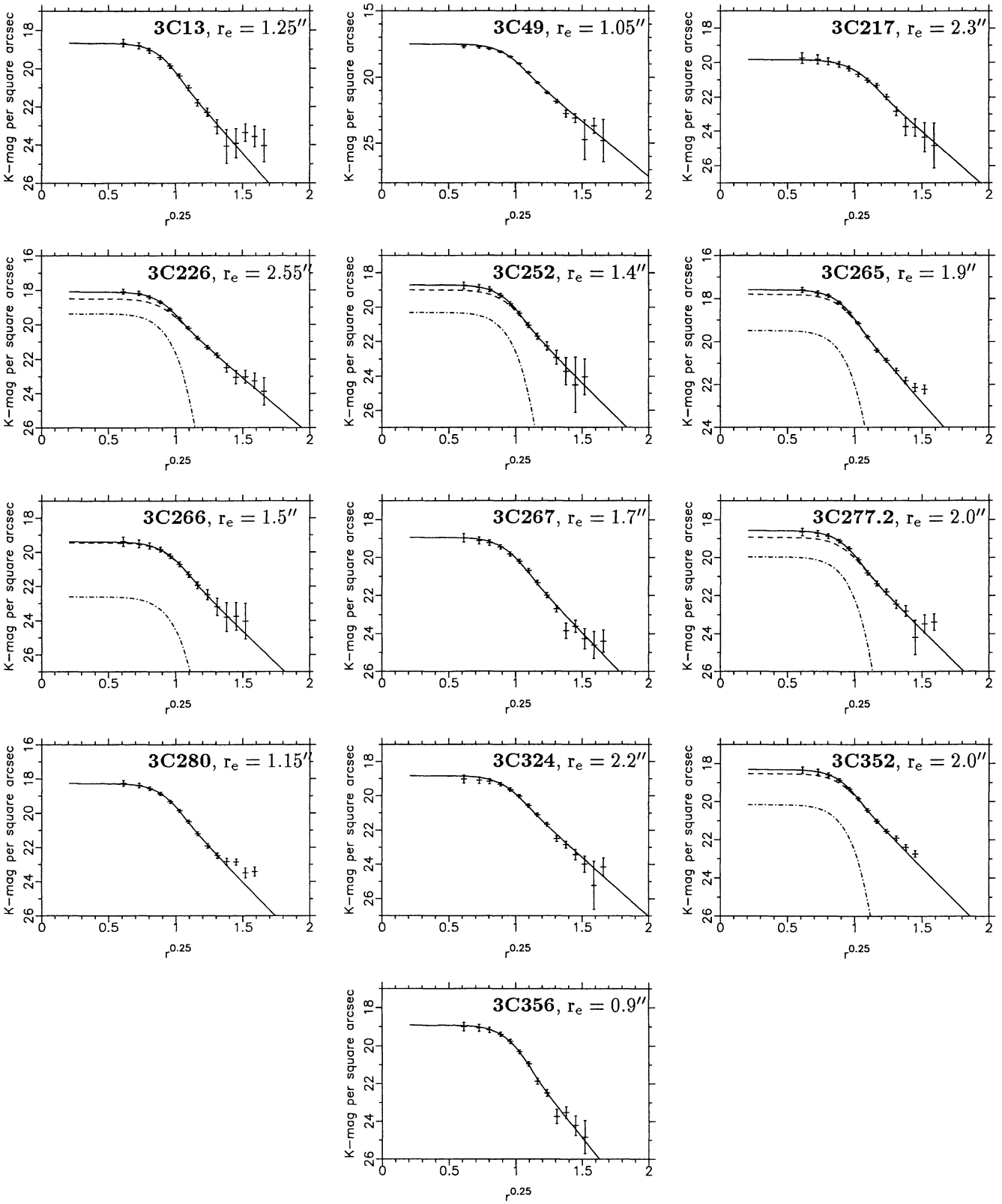

Figure 7. Fits to the radial intensity profiles of the *K*-band images of the 13 3CR galaxies for which de Vaucouleurs profiles could not be determined from the *HST* observations. The characteristic radii have been determined from the best-fitting profiles. The same notation is used as in Fig. 5.

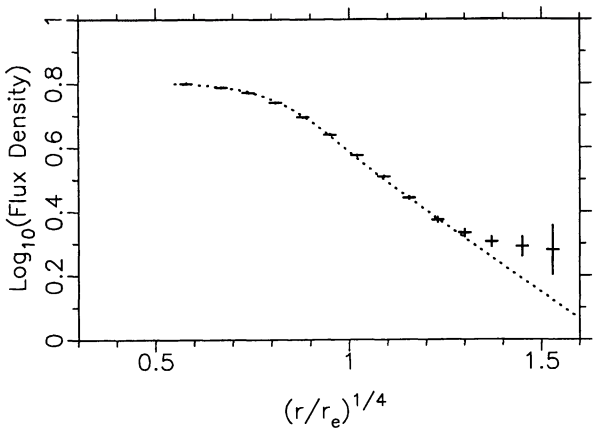

Figure 8. A combined radial intensity profile in the K band for the 12 galaxies with $1.0 \leq r_e \leq 2.0$. Units on the y-axis are arbitrary. The combined errors for each point are shown. The dotted line shows a combined de Vaucouleurs profile: halo emission is clearly visible at $r \gtrsim 2.5r_e$ [i.e. $(r/r_e)^{1/4} \gtrsim 1.25$].

derived for the 3CR galaxies. Fig. 8 strongly suggests that at least some of the 3CR galaxies at redshifts $z \gtrsim 1$ are cD galaxies in rich cluster environments.

5 SURFACE PHOTOMETRY AND COMPARISON WITH LOW-REDSHIFT ELLIPTICAL GALAXIES

Elliptical galaxies at low redshift possess spectrophotometric properties that lie on the 'fundamental plane', in which their characteristic radii r_e, average surface brightnesses within their characteristic radius $\langle\mu\rangle_e$, and velocity dispersions σ_v are strongly correlated. The projection of the fundamental plane using only r_e and $\langle\mu\rangle_e$, known as the Kormendy relation, also produces a tight correlation and avoids the need for detailed spectroscopy (Kormendy 1977; Schombert 1987; Oegerle & Hoessel 1991). This provides a powerful tool for investigating the stellar populations of high-redshift elliptical galaxies.

To compare the 3CR galaxies with existing data for elliptical galaxies at low redshift, the mean rest-frame V-band surface brightnesses within the de Vaucouleurs radii are required. Although in many cases an *HST* image at rest-frame V band is available, these are dominated by the flat-spectrum aligned component, and may also be influenced by dust extinction. As shown above, however, the K-band images are relatively unaffected except in a few cases; in the analysis that follows we omit 3C 22 and 3C 41 because of the presence of nuclear components which contribute to their K-band emission.

We adopt the same assumptions as in Section 3, namely that the 3CR radio galaxies are passively evolving giant elliptical galaxies which formed at a large redshift, with an additional flat-spectrum aligned component. We use the results of Section 3 to remove the contributions of any flat-spectrum or nuclear component from the K-band flux densities of the galaxies. The K-band surface brightnesses thus derived are listed in Table 2. The Bruzual & Charlot (1993) stellar synthesis codes were used to produce the SED of a passively evolving elliptical galaxy, which formed at $z_f = 10$, at the redshift of each 3CR source. These SEDs were then used to derive appropriate K corrections and hence, taking account of the $(1+z)^4$ cosmological surface brightness dimming, the mean rest-frame V-band surface brightnesses. The variation of the V-band flux density with age for each synthesized galaxy was determined, and was used to convert the derived V-band surface brightness into that which would be observed when the galaxy had continued to evolve passively through to zero redshift. This procedure resulted in surface brightnesses of the 3CR galaxies that can be compared directly with low-redshift giant ellipticals in the fundamental plane.

The derived surface brightnesses are included in Table 2, and are plotted against the de Vaucouleurs radius in Fig. 9 (solid circles),

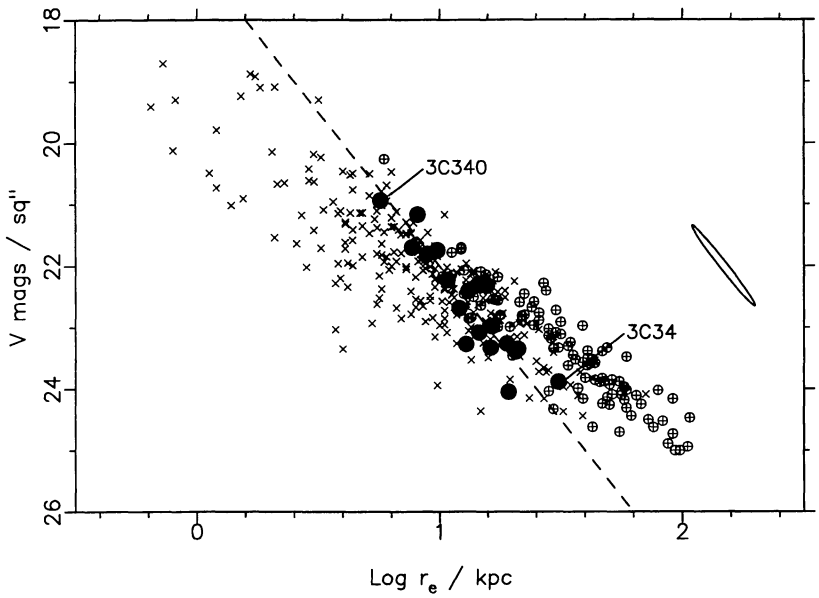

Figure 9. The V-band Kormendy relation for the 3CR galaxies (solid circles) compared with low-redshift ellipticals (crosses) and brightest cluster galaxies (crossed circles). The low-redshift data are from Schombert (1987). The V magnitude data of the 3CR galaxies refer only to the stellar components, and have been derived from their K magnitudes assuming that the stellar populations evolve passively. The ellipse indicates the error ellipse for the 3CR galaxies for which characteristic radii were measured from the UKIRT data; those for which the measurements were obtained from the *HST* data have error ellipses less than half this size. The dashed line shows a line of constant total luminosity.

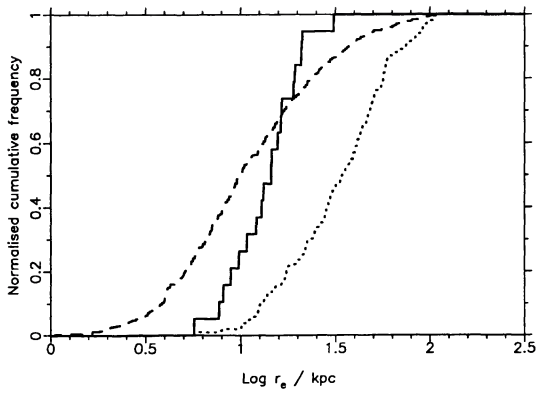

Figure 10. Normalized cumulative frequency distributions of r_e for the three different populations of galaxies: solid line – the high-redshift 3CR galaxies; dotted line – low-redshift brightest cluster galaxies; dashed line – low-redshift elliptical galaxies (excluding brightest cluster galaxies). The 3CR galaxies have a much smaller spread in r_e than the low-redshift elliptical galaxies.

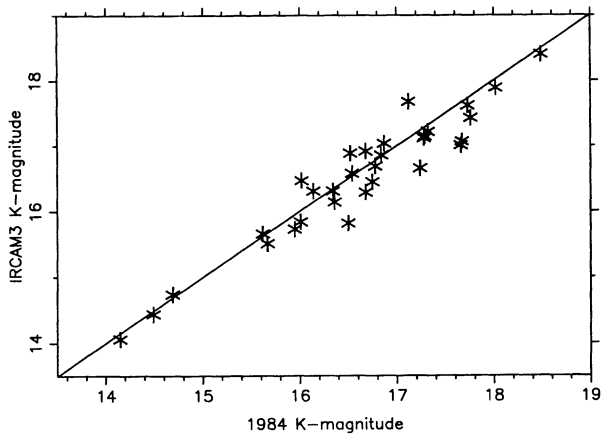

Figure 11. A plot of the K magnitudes measured for the 28 3CR sources in the recent IRCAM3 observations against those of Lilly & Longair (1984). In the diagram, the new K magnitudes were reduced to the same apertures as used by Lilly & Longair in their single-element photometry. Most of the discrepancies are within the quoted errors on the original observations, but there are a few significant changes.

together with data from low-redshift samples of brightest cluster galaxies in Abell clusters (crossed circles) and other ellipticals (crosses) taken from Schombert (1987). The radio galaxies lie along the fundamental plane defined by the low-redshift ellipticals, providing direct evidence that their stellar populations indeed formed at large redshifts and are passively evolving. The SEDs, and hence the K corrections, of either young or non-evolving stellar populations would be significantly different and the 3CR galaxies would not lie on the Kormendy relation.

There is some evidence that the slope of the Kormendy relation defined by the 3CR galaxies is slightly steeper than that of the low-redshift ellipticals. The dashed line in Fig. 9 shows a line of constant total luminosity, that is, a line along which the product of the surface brightness and the square of the characteristic radius is constant. The 3CR galaxies lie roughly along such a line, suggesting that, if they all evolved passively until a redshift of zero, the resultant galaxies would have similar luminosities. This result is similar to that found by Lilly & Longair (1984), and the inclusion of the surface brightness information in Fig. 9 confirms that the radio galaxies at $z \sim 1$ are old giant elliptical galaxies. It seems that the powerful 3CR radio sources are only formed if their host galaxies attain a specific well-defined stellar mass. We return to this point in Section 7.

The data in Fig. 9 can be used to compare the range of values of r_e of the high-redshift 3CR galaxies with those of the populations of low-redshift brightest cluster galaxies and of other ellipticals. Normalized cumulative frequency distributions of r_e for each of the three samples in Fig. 9 are plotted in Fig. 10. Two differences are apparent: first, the dispersion of r_e in the 3CR galaxies is significantly smaller than that of the other two populations; secondly, the mean characteristic radius of the high-redshift 3CR galaxies ($\overline{r_e} = 14.6 \pm 1.4$ kpc) is greater than that of the low-redshift ellipticals ($\overline{r_e} = 8.2 \pm 1.0$ kpc), but about a factor of 2.25 smaller than that of the low-redshift brightest cluster galaxies ($\overline{r_e} = 32.7 \pm 1.1$ kpc). It should be noted that the characteristic sizes of the distant 3CR radio galaxies are dependent upon the adopted value of q_0 and, for $q_0 = 0$, would be approximately 25 per cent smaller. On the other hand, the small degeneracy between the detection of a point-source component and the value of the characteristic radius, discussed in Section 4, means that if there were to be a small nuclear contribution to these galaxies then the characteristic radii would be up to 20 per cent larger than those derived. Neither of these effects would change the significance of the results.

According to cannibalism models (e.g. Hausman & Ostriker 1978) the position of a galaxy along the fundamental plane is interpreted as being related to its merger history. Assuming that the mergers occur homologously (e.g. Schombert 1987 and references therein), when a small galaxy is cannibalized by a much larger galaxy to produce a bound remnant, a large fraction of the kinetic energy of the merger is converted into binding energy of the remnant. The result of such a homologous merger is that the remnant has a larger radius and more diffuse morphology as compared with the original galaxy, thus moving the galaxy to the right along the projected fundamental plane in Fig. 9 (Hausman & Ostriker 1978). In this respect, the larger size of the high-redshift 3CR galaxies as compared with low-redshift elliptical galaxies is important: despite being observed at a much earlier cosmic epoch, the 3CR galaxies at $z \sim 1$ appear to be highly evolved dynamically. We discuss the relative sizes of the distant 3CR galaxies and the brightest cluster galaxies in Section 7.

Within the 3CR sample, it is interesting that 3C 34 has the largest characteristic radius, suggesting that it has undergone most mergers, whilst 3C 340 is the most compact object. The former of these is known to lie towards the centre of a moderately rich cluster of galaxies (McCarthy 1988; Best, Longair & Röttgering 1997a), whilst there is practically no depolarization of the radio lobes of the latter (Johnson, Leahy & Garrington 1995), suggesting that there is relatively little cluster gas surrounding the galaxy.

6 THE REVISED K–z DIAGRAM

Much evidence has been presented in the previous sections confirming the stellar nature of the infrared emission of the galaxies that host the 3CR radio sources. A revised K–z relation for the 3CR galaxies has been derived, including a number of improvements over the original version presented by Lilly & Longair (1984).

(i) The K magnitudes measured by Lilly & Longair were obtained by single-element aperture photometry using blind offsets

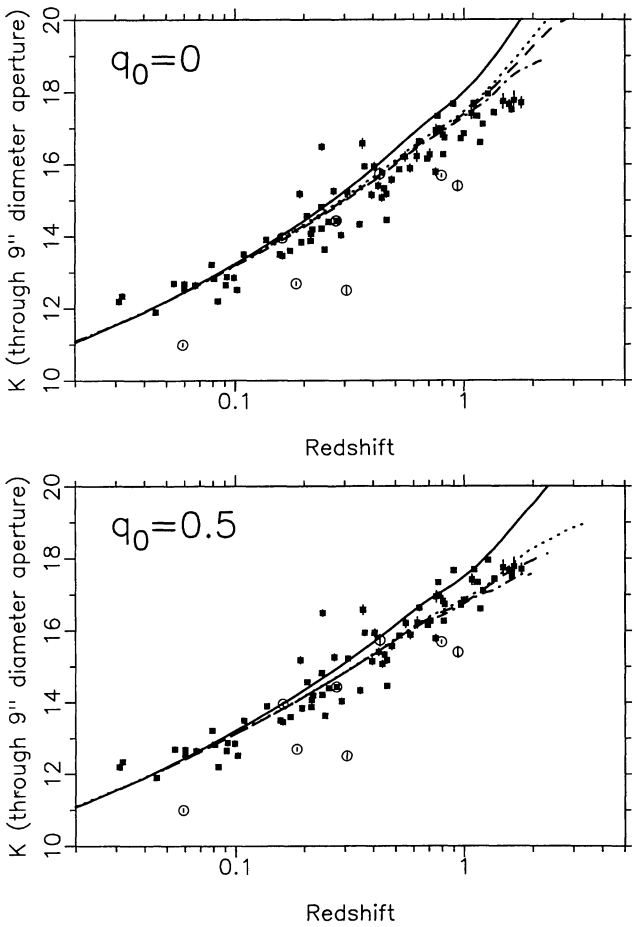

Figure 12. Plots of K magnitude versus redshift for the 3CR radio galaxies. Broad-line radio galaxies are marked by open circles as are 3C 22 and 3C 41, and narrow-line radio galaxies by filled squares. The error in the K magnitude measurements is indicated by the vertical error bar associated with each point; in many cases, this is smaller than the plotted symbol. The upper plot corresponds to $q_0 = 0$ and the lower plot to $q_0 = 0.5$. The lines on each plot show the predicted K–z tracks of various evolutionary models and have been reduced to the magnitudes observed within a 9 arcsec diameter aperture at each redshift. The solid lines correspond to a non-evolving stellar population, whilst the dotted, dashed and dash–dotted lines are for passively evolving galaxies formed at z_f =20, 5 and 3 respectively. The theoretical curves are normalized to match the low-redshift ($z \lesssim 0.1$) narrow-line radio galaxies.

and chopping. The new magnitudes show that, although in the majority of cases the 1984 infrared magnitudes were remarkably accurate, in a small number of cases the on-source apertures were sufficiently large to contain emission from companions, or the off-source reference beam included a faint object (Fig. 11). The new imaging infrared observations allow these problems to be eliminated.

(ii) Lilly & Longair had to make significant aperture corrections for many of the high-redshift radio galaxies; in most cases, our magnitudes were measured through the adopted 9 arcsec diameter aperture. Any extended haloes are generally only present at a radius $r \gtrsim 35$ kpc (4 arcsec at $z \sim 1$), and so the contribution of any halo to the total K-band flux density within the 9 arcsec diameter aperture adopted for our photometry is unimportant.

(iii) The sources 3C 22 and 3C 41 are not included with the narrow-line galaxies, but are classified with the broad-line galaxies in which a nuclear component makes a significant contribution to the K-band flux density.

(iv) The contribution of the aligned component to the K-band magnitude has been removed by subtracting the appropriate fraction of flux density as estimated by our SED fitting in Section 3.1. The fraction of the total flux density that might be associated with any point-source component has also been removed. The combination of these two corrections generally amounts to less than 20 per cent, corresponding to about 0.2 mag. The corrected K_{corr} magnitudes are listed in Table 1.

For the radio galaxies with redshifts $z < 0.6$, the photometry of Lilly & Longair (1984) was adopted. These galaxies are sufficiently bright that offsetting on to nearby faint companions would have had only a small effect upon the observed magnitudes, and there is no evidence for a strong alignment effect at low redshifts. The magnitudes of these galaxies have all been scaled to a 9 arcsec diameter aperture, using a radial light profile appropriate for low-redshift radio galaxies (e.g. Lilly, McLean & Longair 1984): the corrections required are small, being less than 0.3 mag in all cases, and generally less than 0.1 mag.

The revised K–z relation is shown in Fig. 12. The broad-line radio galaxies, together with 3C 22 and 3C 41, are plotted as open circles. The predicted K–z tracks for various evolutionary models and cosmological parameters are also shown, normalized to match the low-redshift ($z \lesssim 0.1$) narrow-line radio galaxies. These tracks include a correction based upon a standard radial light curve for low-redshift giant elliptical galaxies, to account for the fact that the galaxies are observed through an aperture of fixed angular size of 9 arcsec, rather than fixed physical size. At redshifts $z \sim 1$, generally over 90 per cent of the flux density is contained within this aperture.

The upper plot of Fig. 12 shows a set of tracks for a $q_0 = 0$ universe, whilst the lower plot shows the corresponding tracks in a $q_0 = 0.5$ universe, in both cases the cosmological constant Λ being taken to be zero. In each case, the solid line represents the track of a non-evolving giant elliptical galaxy, obtained by redshifting the spectrum of a giant elliptical galaxy at the present epoch. The dashed, dotted and dash–dotted lines show the predicted tracks of passively evolving galaxies formed in a 1-Gyr burst at three different redshifts. A good fit to the data is obtained by the passively evolving models in the $q_0 = 0.5$ universe. Little difference is found if the galaxies formed at redshift $z = 5$ or 20, but at redshifts $z \gtrsim 1.2$ the predicted track for galaxy formation at $z = 3$ is significantly brighter than the observed data, indicating that the stellar populations formed at an earlier cosmic epoch. None of the tracks in the $q_0 = 0$ plot provides a good fit to the observations.

7 DISCUSSION

7.1 The cluster environments of the distant 3CR radio galaxies

The amplitudes of the spatial cross-correlation functions for galaxies in the vicinity of nearby 3CR FR II class radio sources (Fanaroff & Riley 1974) are similar to those for normal elliptical galaxies (Prestage & Peacock 1988), whilst the host radio galaxies themselves have optical luminosities and characteristic sizes significantly less than those of first-ranked Abell cluster galaxies (Lilly & Prestage 1987). This indicates that low-redshift FR II sources typically lie in isolated environments or small groups. In contrast, measures of the galaxy cross-correlation function (Yates, Miller & Peacock 1989) and an Abell clustering classification (Hill & Lilly 1991) both indicate that 3CR galaxies with intermediate redshifts,

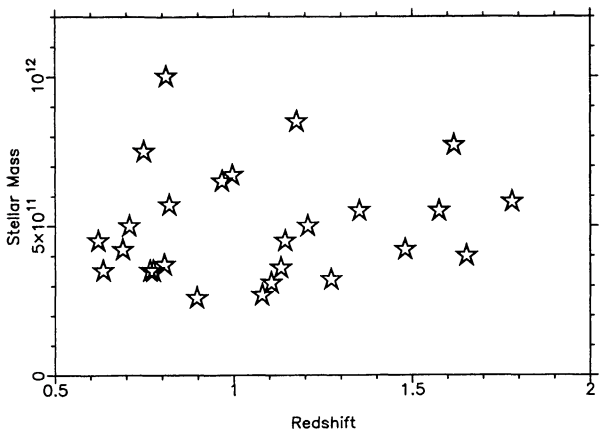

Figure 13. A plot of the stellar mass derived by a fit to the broad-band photometry of Section 3 against redshift for 26 3CR galaxies.

$0.3 \lesssim z \lesssim 0.5$, belong to environments that are about three times richer than those nearby.

There is evidence that the high-redshift 3CR sources belong to moderate to rich cluster environments – in particular: the detection of X-ray emission, in some cases resolved, from a number of these sources has been associated with a cooling flow in a relatively dense intracluster medium (Crawford & Fabian 1993, 1995, 1996; Worrall et al. 1994; Dickinson 1997); companion galaxies are seen around a number of the radio galaxies in the narrow-line [O II] 3727 imaging by McCarthy (1988); infrared imaging of distant radio galaxies provides large numbers of cluster candidates, based upon selection by colour, and spectroscopic follow-up of individual 3CR radio galaxies indeed shows them to lie in at least moderately rich clusters (e.g. Dickinson 1997); a surrounding medium of fairly high density is required to account for the large rotation measures of distant radio sources, and to provide a working surface for their high radio luminosities (Carilli et al. 1997; Best et al. 1998).

In this paper we have provided further evidence in support of this hypothesis. In Section 4 we showed that at least some of these galaxies possess haloes characteristic of those seen around cD galaxies at low redshifts. Furthermore, the stellar masses of the 3CR galaxies derived in Section 3.1 indicate that they are amongst the most massive galaxies at the cosmic epochs at which they are observed. A comparison of the 3CR galaxies with the brightest cluster galaxy (BCG) sample of Aragón-Salamanca et al. (1993) shows that the absolute K magnitudes, and hence stellar masses, of the two samples at redshift $z \sim 1$ are essentially the same. In contrast, at low redshifts, BCGs are about a magnitude brighter than the 3CR radio galaxies in absolute K-magnitude, consistent with the result that low-redshift 3CR galaxies lie in isolated environments of small groups. This difference is best illustrated by the fact that the K–z relation of the BCGs is consistent with non-evolving stellar populations (Aragón–Salamanca et al. 1993).

To understand the K–z relations, we must therefore unravel two 'cosmic conspiracies'.

(i) On the one hand, the tightness and slope of the 3CR K–z relation suggest that the radio galaxies belong to a single population of objects which formed at large redshift and evolved passively over the redshift interval $2 > z > 0$, such that a high-redshift 3CR galaxy would evolve into a low-redshift 3CR galaxy. This simple picture cannot be correct because we have argued that the galactic environments of FR II 3CR radio galaxies change with redshift. High-redshift 3CR galaxies appear to lie in (proto-)cluster environments, whilst the nearby sources in the sample are found in isolated environments or small groups.

(ii) On the other hand, the K–z relation of the BCGs suggests that their stellar populations are non-evolving, but this is clearly an unphysical picture. All passively evolving models for stellar populations suggest that they should be about a magnitude brighter in absolute K magnitude at redshift $z = 1$ as compared with $z = 0$.

Since the stellar populations of the BCGs must have evolved in the same way as the 3CR radio galaxies, the shape of their K–z relation reflects the fact that central cluster galaxies continue to accumulate matter through mergers and gas infall. Hierarchical clustering models for structure formation have suggested that the mass of BCGs can increase by a factor of up to 5 between a redshift of 1 and the present epoch (Aragón-Salamanca, Baugh & Kauffman 1998). In contrast, the variation of the stellar masses of the 3CR galaxies with redshift, as derived from the SED fits of Section 3.1, shows no correlation (see Fig. 13).

In Section 5 we showed that the mean characteristic radius of the distant 3CR radio galaxies was approximately a factor of 2.25 smaller than that of the nearby BCGs. Kormendy (1977) derived a relation between the integrated luminosity of a bright elliptical galaxy and its characteristic radius: $L_{\rm int} \propto r_{\rm e}^{0.7}$, or, equivalently, $M_{\rm stel} \propto (M/L)_0 r_{\rm e}^{0.7}$, where $M_{\rm stel}$ is the stellar mass of the galaxies and $(M/L)_0$ is the mass-to-light ratio of the stellar populations at redshift zero. This result was confirmed for elliptical galaxies with $r_{\rm e} \gtrsim 6$ kpc by Schombert (1987). This implies that the stellar masses of the 3CR radio galaxies at redshift $z \sim 1$ are only a factor of about 1.75 below those of nearby central galaxies in Abell clusters, assuming that their stellar populations will have a similar mass-to-light ratio when they have evolved to redshift zero. When compared with the growth factor of between 3 and 5 expected for BCGs over this redshift interval, it is clear that the distant 3CR galaxies are massive galaxies, even relative to the progenitors of the central galaxies of rich clusters.

Intriguingly, West (1994) has shown that the comoving number density of the host galaxies of powerful high-redshift radio sources is of the same order of magnitude as that of rich Abell clusters, if account is taken of the fact that radio source lifetimes, $\sim 10^8$ yr, are much shorter than the age of the Universe. It is quite conceivable that all of the brightest galaxies in clusters today went through a phase during which they were intense radio sources, and so must possess supermassive black holes in their nuclei (e.g. van der Marel et al. 1997 and references therein).

7.2 Understanding the 3CR radio galaxies

Since 3CR radio galaxies at large redshifts lie at the centres of galaxy clusters, their masses would be expected to increase with cosmic epoch just like the BCGs; the 'passively evolving' K–z relation of these galaxies suggests, however, that this does not occur. This is a conspiracy: the galaxies sampled at high and low redshifts do not form a uniform population, as is indicated by the dramatic change in their galactic environments with redshift. To understand this effect, we compare the K–z relation of the 3CR galaxies with that of the only other complete sample of low-frequency-selected radio sources, the 6C radio galaxies (Eales & Rawlings 1996; Eales et al. 1997). There are important differences between the two samples, specifically:

(i) at a given redshift, the 3CR radio sources are about a factor of

5 more powerful than the 6C radio sources, since the latter are selected from a fainter radio survey;

(ii) at low redshifts, $z \lesssim 0.6$, the 3CR and 6C radio galaxies have similar infrared luminosities;

(iii) at redshifts $z \sim 1$, the (un-corrected) K-band luminosities of the 3CR galaxies are greater than those of the 6C galaxies by, on average, 0.6 mag (Eales et al. 1997), although there is significant overlap between the two populations.

Points (ii) and (iii) reflect the fact that the K–z relation for 6C radio galaxies is consistent with a non-evolving population of radio galaxies (Eales & Rawlings 1996).

Three possible reasons why the K magnitudes of the 3CR galaxies might be brighter than those of the 6C galaxies at $z \gtrsim 1$ are: (i) there may be a strong direct or indirect AGN contribution to the K-band emission of the high-redshift 3CR galaxies (e.g. Eales et al. 1997); (ii) the 3CR galaxies may be younger than the 6C galaxies, and hence their stellar populations may be more luminous; (iii) the 3CR galaxies may be more massive than the 6C galaxies and thus contain a greater number of stars.

Concerning the first possibility, nearly 50 per cent of the K-band emission of the 3CR galaxies would have to be associated with AGN activity. The results presented in this paper show that, with the exceptions of the two sources 3C 22 and 3C 41, the mean point-source contribution to the total K-band flux density is only 4 per cent, with secure upper limits of $\leq$15 per cent. We have discussed why line emission from gas excited by the AGN light is unlikely to be important, and have estimated the mean contribution of the aligned emission to the K-band flux density to be about 10 per cent. We conclude, therefore, that the sum of these effects will contribute at most about 0.3 of the 0.6-mag difference between the two samples.

In the second case, if the 3CR galaxies were formed at a smaller redshift than the 6C galaxies, say $z_f \sim 2.5$, their younger stellar populations would be more luminous than the corresponding 6C galaxies at redshifts $z \gtrsim 1$, but by $z \sim 0.6$ they would have aged and the galaxies would no longer be significantly more luminous. The main objections to this picture are that features detected in the spectra of some of the galaxies, coupled with their very red infrared colours, imply much greater ages for the stellar populations of the 3CR radio galaxies than would be expected in this picture (e.g. Stockton et al. 1995), and that it is difficult to assemble such massive, dynamically evolved systems as the 3CR galaxies in a short cosmic time.

It is likely, therefore, that both the 6C and 3CR populations formed at large redshifts, and that the 6C galaxies are fainter than the 3CR galaxies in the K band at high redshift because they contain, on average, a lower mass of stars. The primary selection criteria for these samples of radio galaxies are the limiting radio flux densities of the 3CR and 6C catalogues, and so the different K–z relations of these two samples imply that the radio luminosities of the sources must depend upon the masses and environments of the host galaxies.

According to conventional ideas about the origin of FR II radio sources, their luminosities are ultimately determined by the powers of the beams of particles ejected by the AGN, and by the density of the surrounding interstellar and intergalactic gas which controls adiabatic radiation losses of the radio lobes. In turn, the intrinsic beam power of the source is determined by the mass of the central black hole, the mass of material accreting on to it, and the efficiency with which this is converted into beam energy. Given an abundant supply of fuel, it is a reasonable assumption that the total energy output of the central engine, which is dominated by the bulk kinetic power of the radio jets (Rawlings & Saunders 1991), will be close to the Eddington limiting luminosity. Rawlings & Saunders derived the total kinetic power of the jets in radio galaxies with redshifts $z \sim 1$ and found values corresponding to the Eddington limiting luminosity of a black hole with a mass of a few times $10^8\,M_\odot$; Kaiser, Dennett-Thorpe & Alexander (1997) suggest that the jet powers may be even higher. Theorists have long argued that the masses of the central black holes should be roughly proportional to the masses of the host galaxies (Soltan 1982; Efstathiou & Rees 1988; Small & Blandford 1992; Haehnelt & Rees 1993), and some evidence for such a correlation has recently been found for massive black holes in the nuclei of nearby galaxies (Kormendy & Richstone 1995). Thus the luminosity of a radio source is determined by three principal factors: the mass of the host galaxy, the availability of fuel, and the density of the environment.

The gas that forms the fuel for radio sources may arise either through the infall of interstellar and intergalactic material towards the central regions of the galaxy, or as a result of an interaction or merger with a gaseous dwarf galaxy (Heckman et al. 1986; Smith & Heckman 1989, 1990; Menon 1992). In high-redshift proto-cluster or young cluster environments, the central galaxies will be massive, and so contain amongst the most powerful central engines at that epoch. There will also be high merger rates and a plentiful supply of disturbed intracluster gas to fuel the central engine and confine the radio lobes. Furthermore, Ellingson, Green & Yee (1991) have found that the velocity dispersions of galaxies around distant powerful radio sources are significantly lower (400 to 500 $\mathrm{km\,s^{-1}}$) than those in comparably rich clusters at low redshifts (500 to 1000 $\mathrm{km\,s^{-1}}$). These smaller relative velocities increase the efficiency of galaxy mergers. Thus massive galaxies in young cluster environments at high redshifts possess all the necessary ingredients for producing the most powerful radio sources.

Radio sources in galaxies of lower mass than the 3CR galaxies are likely to be powered by less massive black holes and therefore to have lower intrinsic beam powers. It is reasonable to attribute the lower radio luminosity of the high-redshift 6C radio sources as compared with the 3CR sources to the fact that the 6C galaxies are less massive and possess less massive black holes. The overlap between the two samples on the K–z relation would then arise from the scatter in the correlation between the stellar mass of the galaxy and the mass of the black hole (e.g. Kormendy & Richstone 1995): for example, a galaxy with a K magnitude comparable to that of the 3CR galaxies, but with a central black hole less massive than predicted by the correlation, would host a 6C radio source.

At redshifts $z < 0.6$, the lower radio luminosity of all radio sources means that the galaxies are no longer producing radio beams with kinetic powers close to the Eddington limit. The analysis of Rawlings & Saunders (1991) confirms that the beam powers of these sources are significantly lower than the values found in the radio galaxies at $z \sim 1$. Neither the masses of individual black holes nor the galaxy clustering can decrease with cosmic epoch, and so the radio luminosities of low-redshift sources must be limited not by the mass of the host galaxy, as are high-redshift sources, but rather by the availability of gas in the host galaxy and its environment to fuel the central black hole. As a result, at low redshift a weaker correlation would be expected between galaxy mass and radio luminosity. This may account for the similarity of the K-band magnitudes of the 3CR and 6C galaxies at these redshifts.

This decrease in the fuelling gas density with cosmic epoch has been argued on different grounds by other authors (e.g. Rees 1990

and references therein). It is also consistent with recent results on the evolution of the fraction of baryons in the form of neutral hydrogen, and the enrichment of the heavy elements, which indicate that the quantity of interstellar and intracluster material has decreased significantly from redshifts $z \sim 2$ to $z = 0$ (Madau et al. 1996).

7.3 Cosmic evolution of the radio source population

We have argued that radio galaxies at high redshifts lie in young cluster environments, and that such environments possess the ideal ingredients for producing powerful radio sources. Why then are the most powerful FR II radio sources at the present epoch not also associated with central cluster galaxies? The radio sources hosted by nearby BCGs are almost invariably 'edge-darkened' FR I type radio sources. FR Is do not possess large luminous radio lobes; instead, the jets are decelerated significantly in the inner kiloparsec, probably as a result of entrainment of external material (Laing 1993, and references therein), implying a relatively low kinetic power for FR I jets. How do the environments of low-redshift central cluster galaxies restrict, in some way, the central engines of these galaxies to producing only the lower power FR I jets?

Narayan & Yi (1995) have shown that if the accretion rate on to a black hole falls below a critical value given by $\dot{M}_{\rm crit} \approx \alpha^2 \dot{M}_{\rm Edd}$ (where α is the viscosity parameter which has a value of order 0.1) then accretion on to the black hole occurs in an advection-dominated mode. At higher accretion rates a radiatively efficient thin accretion disc forms. Studying the core spectra of the radio-loud quasar 3C 273 and the FR I source M87, Reynolds et al. (1996) argue that the difference between FR I and FR II sources may be that the central engines of FR I sources accrete matter at a rate below the critical value. The large difference in jet luminosity between FR I and FR II type sources would then arise from a much smaller difference in the mass accretion rate, coupled with a change in the accretion mechanism.

Baum, Heckman & van Breugel (1992) showed that the gas surrounding FR I radio galaxies is of low angular momentum, with no evidence for recent mergers, whilst that surrounding FR II sources is generally of higher angular momentum and frequently exhibits tidal tails or other evidence for mergers. Rich regular clusters at low redshifts have had time to virialize the spatial distribution of the galaxies, and for the intracluster gas to take up an equilibrium configuration within the cluster gravitational potential. Studies of the Butcher–Oemler effect (Butcher & Oemler 1978) indicate that, compared with high-redshift clusters, there is a dearth of gas-rich galaxies close to the centres of low-redshift clusters which might merge with, and fuel, the central galaxy. Furthermore, the high velocity dispersion of the galaxies greatly reduces the merger efficiency. The evolution and virialization of low-redshift clusters are therefore likely to result in a more restricted fuelling supply for the central engines of BCGs, and the fuelling gas may arise solely through steady accretion from the interstellar or intracluster media (see also Baum, Zirbel & O'Dea 1995). The most powerful FR II radio sources at small redshifts are generally found instead in small groups of galaxies: in these groups, velocity dispersions are small, mergers relatively frequent, and gas-rich galaxies plentiful. Occasionally, dramatic mergers will occur in low-redshift BCGs, producing radio sources of comparable radio power to the $z \sim 1$ 3CR sources, and we ascribe exceptional sources such as Cygnus A to this process (see also Barthel & Arnaud 1996).

These considerations suggest an explanation for the constancy of the stellar masses of the 3CR galaxies throughout the redshift range $0.03 \leq z \leq 1.8$. This mass may be interpreted as the typical mass that a giant elliptical galaxy attains before its galactic and gaseous environment is virialized. Galaxies of mass greater than a few times $10^{11}\,{\rm M}_{\odot}$ will have undergone greater dynamical evolution, and generally live in virialized environments where the reduced supply of fuelling gas to the central regions results in FR I sources being formed. This leads naturally to a correlation between the redshift of a 3CR FR II galaxy and the richness of its environment: galaxies in highly overdense environments accumulate matter the fastest, and therefore reach this 'FR II upper mass limit' at early cosmic epochs, whilst those that lie in less dense environments evolve more slowly and can form powerful FR II radio galaxies at the current epoch.

In the model presented here, the location of the distant 3CR galaxies in the low-redshift fundamental plane can be understood. All galaxies evolve through accumulation of matter and move to the right along the fundamental plane. For a galaxy to form a radio source at $z \sim 1$ of sufficient radio power to be in the 3CR sample, the galaxy (and hence its central black hole) must have attained a certain mass, and therefore a certain luminosity, which is close to the dashed line in Fig. 9. The small scatter in their characteristic radii follows naturally from the galaxies being seen at a similar point in their evolutionary history.

This model is also fully consistent with the redshift evolution of the alignment effect seen in powerful radio galaxies (e.g. McCarthy 1993; Paper III). At high redshifts, the sources lie in environments in which the surrounding gas is unsettled, distributed throughout the forming cluster, and of relatively high density. Most models of the alignment effect depend critically upon the availability of cool gas and so, at intermediate and low redshifts where the environments of the sources have much lower gas densities and the gas is more settled, there is a decrease in the luminosity of aligned emission.

These results suggest that the highest redshift ($z \gtrsim 2$) radio galaxies, like the 3CR galaxies, are amongst the most massive systems at their observed epoch (see also Pentericci et al. 1997). These galaxies must have accumulated their mass at early cosmic epoch, and so must belong to environments in which the most massive systems are formed by a redshift of zero. The dense surrounding environment and the abundant supply of fuel required are consistent with the detection of large Lyα haloes around these objects (e.g. Röttgering & Miley 1996, and references therein), and the very large depolarization and rotation measures of their radio emission (Carilli et al. 1997).

A combination of luminosity evolution of the radio source population, and the greater availability of gas at high redshifts increasing the probability of a powerful radio source being formed, provides a natural explanation for the increase in the comoving number density of radio galaxies and quasars out to redshifts $z \sim 2$. The levelling off and decline in the comoving number density of powerful radio sources with $z > 2$ can plausibly be explained in terms of the fact that systems that are rich enough to produce sufficiently massive host galaxies, and consequently massive enough black holes in their nuclei, had not had time to form by that epoch.

At the same time, these results also provide an explanation of why other populations of active galaxies, such as the optically selected quasars and the bright X-ray galaxies, show the same evolutionary behaviour as the powerful radio galaxies (Dunlop 1994): since the maximum radio luminosity is governed by Eddington-limited accretion, this same process will define the limiting optical and X-ray luminosities. Therefore the cosmic evolution of all classes of active galaxy are governed by the same

two parameters: the evolution of black hole masses, and the decrease in the availability of fuelling gas with cosmic epoch.

8 CONCLUSIONS

The main conclusions of the study of the old stellar populations of these 3CR galaxies are as follows.

(i) The magnitudes, colours and location of the distant 3CR galaxies on the projected fundamental plane for elliptical galaxies indicate that their stellar populations formed at large redshift and are passively evolving. Their spectral energy distributions can be well matched using such an old stellar population together with an aligned component of relatively flat spectrum.

(ii) Except in two cases (3C 22 and 3C 41), there is no evidence for a nuclear point-source contribution to the K-band emission at $\gtrsim$15 per cent of the total flux density at that wavelength.

(iii) At least some of the high-redshift 3CR galaxies possess extended envelopes, similar to the haloes seen around nearby cD galaxies. Such envelopes are not seen around low-redshift 3CR galaxies, indicating a difference between the high- and low-redshift populations. The high-redshift 3CR galaxies appear to live in environments that will form rich clusters by a redshift of zero.

(iv) The 3CR radio galaxies have a similar stellar mass over the complete redshift range of the sample. The less powerful 6C radio sources have lower stellar masses at high redshifts; the black holes associated with these galaxies are likely to be correspondingly less massive, producing proportionally weaker radio sources.

(v) Powerful radio sources are not observed in the most massive galaxies at low redshift. A reduced supply of fuelling gas for the central engines, possibly associated with the lower merger rates and lack of gas-rich galaxies towards the centre of virialized clusters, results in lower luminosity FR I type radio sources being preferentially formed.

(vi) If the 3CR galaxies evolve in the same way as brightest cluster galaxies, then the evolution in the comoving number density of powerful radio sources can be naturally understood. Out to redshifts $z \sim 2$, the comoving number density of powerful radio sources increases through a combination of luminosity and density evolution associated with the greater mass accretion rates and the greater probability of a strong radio source being formed. At redshifts $z \gtrsim 2$, the levelling off and decline of the comoving number density would be due to negative density evolution, associated with the decreasing number of galaxies that lie in environments sufficiently rich for them to have accumulated enough matter to produce a powerful radio source by that epoch.

(vii) The commonly used 'uniform population, closed box' galaxy evolution models are not appropriate for interpretations of the K–z relations. Powerful radio galaxies selected at high and low redshifts have different evolutionary histories, but must contain a similar mass of stars, a few times $10^{11}\,M_{\odot}$, and so conspire to produce the 'passively evolving' K–z relation observed. The apparently simple 'no-evolution' shape of the K–z relation for brightest cluster galaxies and lower power radio galaxies is the result of a further conspiracy in which these galaxies become intrinsically fainter owing to stellar evolution, but also brighten because of mass increase through mergers. The shapes of these relations can be used to provide information about the merger histories of massive galaxies in clusters.

ACKNOWLEDGMENTS

This work is based on observations with the NASA/ESA *Hubble Space Telescope*, obtained at the Space Telescope Science Institute, which is operated by AURA Inc., under contract from NASA. The National Radio Astronomy Observatory is a facility of the National Science Foundation, operated under cooperative agreement by Associated Universities Inc. The United Kingdom InfraRed Telescope is operated by the Joint Astronomy Centre on behalf of PPARC. HJAR acknowledges support from an EU twinning project, a programme subsidy granted by the Netherlands Organization for Scientific Research (NWO) and a NATO research grant. This work was supported in part by the Formation and Evolution of Galaxies network set up by the European Commission under contract ERB FMRX- CT96-086 of its TMR programme. We thank the referee for a number of useful comments and suggestions.

REFERENCES

Aragón-Salamanca A., Ellis R. S., Couch W. J., Carter D., 1993, MNRAS, 262, 764
Aragón-Salamanca A., Baugh C. M., Kauffmann G., 1998, MNRAS, in press
Baker J. C., Hunstead R. W., 1996, ApJ, 452, L95
Barthel P. D., Arnaud K. A., 1996, MNRAS, 283, L45
Baum S. A., Heckman T. M., van Breugel W. J. M., 1992, ApJ, 389, 208
Baum S. A., Zirbel E. L., O'Dea C. P., 1995, ApJ, 451, 88
Best P. N., Longair M. S., Röttgering H. J. A., 1997a, MNRAS, 286, 785
Best P. N., Longair M. S., Röttgering H. J. A., 1997b, MNRAS, 292, 758 (Paper I)
Best P. N., Carilli C. L., Garrington S. T., Longair M. S., Röttgering H. J. A., 1998, MNRAS, in press
Bruzual G., Charlot S., 1993, ApJ, 405, 538
Burstein D., Heiles C., 1982, AJ, 87, 1165
Butcher H. R., Oemler A., 1978, ApJ, 219, 18
Calzetti D., Bohlin R. C., Gordon K. D., Witt A. N., Bianchi L., 1995, ApJ, 446, L97
Carilli C. L., Röttgering H. J. A., van Ojik R., Miley G. K., van Breugel W. J. M., 1997, ApJS, 109, 1
Chambers K. C., Miley G. K., van Breugel W. J. M., 1987, Nat, 329, 604
Cimatti A., Dey A., van Breugel W., Antonucci R., Spinrad H., 1996, ApJ, 465, 145
Cimatti A., Dey A., van Breugel W., Hurt T., Antonucci R., 1997, ApJ, 476, 677
Crawford C. S., Fabian A. C., 1993, MNRAS, 260, L15
Crawford C. S., Fabian A. C., 1995, MNRAS, 273, 827
Crawford C. S., Fabian A. C., 1996, MNRAS, 282, 1483
de Koff S., Baum S. A., Sparks W. B., Biretta J., Golombek D., Macchetto F., McCarthy P., Miley G. K., 1996, ApJS, 107, 621
de Vaucouleurs G., Buta R., 1983, AJ, 88, 939
Dey A., Spinrad H., 1996, ApJ, 459, 133
Dey A., van Breugel W. J. M., Vacca W. D., Antonucci R., 1997, ApJ, 490, 698
di Serego Alighieri S., Cimatti A., Fosbury R. A. E., 1994, ApJ, 431, 123
Dickinson M., 1997, in Tanvir N. R., Aragón-Salamanca A., Wall J. V., eds, *HST* and the high redshift Universe. World Scientific, Singapore, p. 207
Dickinson M., Dey A., Spinrad H., 1996, in Hippelein H., Meisenheimer K., Röser H.-J., eds, Galaxies in the Young Universe. Springer Verlag, p. 164
Dickson R., Tadhunter C., Shaw M., Clark N., Morganti R., 1995, MNRAS, 273, L29
Dunlop J. S., 1994, in Wamsteker W., Longair M. S., Kondo Y., eds, Frontiers of Space & Ground-based Astronomy. Kluwer, Dordrecht, p. 395
Dunlop J. S., Peacock J., 1993, MNRAS, 263, 936
Dunlop J. S., Peacock J., Spinrad H., Dey A., Jimenez R., Stern D., Windhorst R., 1996, Nat, 381, 581
Eales S., 1992, ApJ, 397, 49
Eales S. A., Rawlings S., 1996, ApJ, 460, 68

Eales S., Rawlings S., Law-Green D., Cotter G., Lacy M., 1997, MNRAS, 291, 593
Economou F., Lawrence A., Ward M. J., Blanco P. R., 1995, MNRAS, 272, L5
Efstathiou G., Rees M., 1988, MNRAS, 230, 5P
Eisenhardt P., Chokshi A., 1990, ApJ, 351, L9
Ellingson E., Green R. F., Yee H. K. C., 1991, ApJ, 378, 476
Fanaroff B. L., Riley J. M., 1974, MNRAS, 167, 31P
Giavalisco M., Livio M., Bohlin R. C., Macchetto F. D., Stecher T. P., 1996, AJ, 112, 369
Haehnelt M. G., Rees M. J., 1993, MNRAS, 263, 168
Hausman M. A., Ostriker J. P., 1978, ApJ, 224, 320
Heckman T. M., Smith E. P., Baum S. A., van Breugel W. J. M., Miley G. K., Illingworth G. D., Bothun G. D., Balick B., 1986, ApJ, 311, 526
Hill G. J., Lilly S. J., 1991, ApJ, 367, 1
Johnson R. A., Leahy J. P., Garrington S. T., 1995, MNRAS, 273, 877
Kaiser C. R., Dennett-Thorpe J., Alexander P., 1997, MNRAS, 292, 723
Kormendy J., 1977, ApJ, 217, 406
Kormendy J., Richstone D., 1995, ARA&A, 33, 581
Lacy M., Rawlings S., Eales S., Dunlop J. S., 1995, MNRAS, 273, 821
Laing R. A., 1993, in Burgarella D., Livio M., O'Dea C. P., eds, Astrophysical Jets. Cambridge Univ. Press, Cambridge, p. 95
Laing R. A., Riley J. M., Longair M. S., 1983, MNRAS, 204, 151
Lilly S. J., 1989, ApJ, 340, 77
Lilly S. J., Longair M. S., 1982, MNRAS, 199, 1053
Lilly S. J., Longair M. S., 1984, MNRAS, 211, 833
Lilly S. J., Prestage R. M., 1987, MNRAS, 225, 531
Lilly S. J., McLean I. S., Longair M. S., 1984, MNRAS, 209, 401
Madau P., Ferguson H. C., Dickinson M. E., Giavalisco M., Steidel C. C., Fruchter A., 1996, MNRAS, 283, 1388
McCarthy P. J., 1988, PhD thesis, University of California, Berkeley
McCarthy P. J., 1993, ARA&A, 31, 639
McCarthy P. J., van Breugel W. J. M., Spinrad H., Djorgovski S., 1987, ApJ, 321, L29
Menon T. K., 1992, MNRAS, 255, 41
Narayan R., Yi I., 1995, ApJ, 452, 710
Oegerle W. R., Hoessel J. G., 1991, ApJ, 375, 15
Oemler A., 1976, ApJ, 209, 693
Pentericci L., Röttgering H. J. A., Miley G. K., Carilli C. L., McCarthy P. J., 1997, A&A, 326, 580
Prestage R. M., Peacock J. A., 1988, MNRAS, 230, 131
Rawlings S., Saunders R., 1991, Nat, 349, 138
Rawlings S., Eales S., Lacy M., 1991, MNRAS, 251, 17P
Rawlings S., Lacy M., Sivia D. S., Eales S. A., 1995, MNRAS, 274, 428
Rees M. J., 1989, MNRAS, 239, 1P
Rees M. J., 1990, Sci, 247, 817
Reynolds C. S., Di Matteo T., Fabian A. C., Hwang U., Canizares C. R., 1996, MNRAS, 283, L111
Rigler M. A., Lilly S. J., Stockton A., Hammer F., Le Fèvre O., 1992, ApJ, 385, 61
Röttgering H. J. A., Miley G. K., 1996, in Bergeron J., ed., The Early Universe with the VLT. Springer Verlag, p. 285
Scalo J. M., 1986, Fundam. Cosmic Phys., 11, 1
Schombert J. M., 1987, ApJS, 64, 643
Small T. A., Blandford R. D., 1992, MNRAS, 259, 725
Smith E. P., Heckman T. M., 1989, ApJ, 341, 658
Smith E. P., Heckman T. M., 1990, ApJ, 348, 38
Soltan A., 1982, MNRAS, 200, 115
Stockton A., Kellogg M., Ridgway S. E., 1995, ApJ, 443, L69
Tadhunter C. N., Dickson R. D., Shaw M., 1996, MNRAS, 281, 591
Thuan T. X., Romanishin W., 1981, ApJ, 248, 439
van der Marel R. P., de Zeeuw P. T., Rix H. W., Quinlan G. D., 1997, Nat, 385, 610
West M. J., 1991, ApJ, 379, 19
West M. J., 1994, MNRAS, 268, 79
Worrall D. M., Lawrence C. R., Pearson T. R., Readhead A. C. S., 1994, ApJ, 420, L17
Yates M. G., Miller L., Peacock J. A., 1986, MNRAS, 221, 311
Yates M. G., Miller L., Peacock J. A., 1989, MNRAS, 240, 129

This paper has been typeset from a TEX/LATEX file prepared by the author.